Gravitational Lensing by a Dark Compact Object in Modified Gravity

By

Nagina Rehman

(Registration No: 00000403037)

A thesis submitted in partial fulfillment of the requirements for the degree of

Master of Philosophy in

Mathematical Sciences

Supervisor: Dr. Mubasher Jamil

School of Natural Sciences

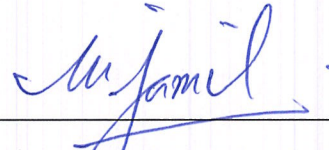National University of Sciences and Technology (NUST)

Islamabad, Pakistan

(2024)

THESIS ACCEPTANCE CERTIFICATE

Certified that final copy of MS thesis written by **Nagina Rehman** (Registration No **00000403037)**, of **School of Natural Sciences** has been vetted by undersigned, found complete in all respects as per NUST statutes/regulations, is free of plagiarism, errors, and mistakes and is accepted as partial fulfillment for award of MS/M.Phil degree. It is further certified that necessary amendments as pointed out by GEC members and external examiner of the scholar have also been incorporated in the said thesis.

Signature: _____

Name of Supervisor: Prof. Mubasher Jamil_____

Date: _____13—12—2024_____

Signature (HoD): _____

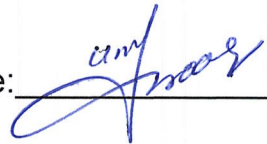Date: _____17—12—2024_____

Signature (Dean/Principal): _____

Date: _____17·12·2024_____

National University of Sciences & Technology

MS THESIS WORK

We hereby recommend that the dissertation prepared under our supervision by: <u>Nagina Rehman,</u> Regn No. <u>00000403037</u> Titled <u>Gravitational Lensing by Dark Compact Objects in Modified Gravity</u> be Accepted in partial fulfillment of the requirements for the award of MS degree.

Examination Committee Members

1. Name: <u>PROF. AZAD A. SIDDIQUI</u>   Signature:_____

2. Name: <u>PROF. MUHAMMAD UMER FAROOQ</u>   Signature:_____

Supervisor's Name <u>PROF. MUBASHER JAMIL</u>   Signature:_____

_____
Head of Department

17-12-2024
Date

COUNTERSINGED

Date: 17.12.2024

_____
Dean/Principal

Acknowledgement

Contents

IV

List of Tables

List of Figures

X

Abstract

This study investigates gravitational lensing in modified gravity theories, focusing on the lensing phenomenon in strong and weak gravitational fields. We derive the weak bending angle of light using modified gravity spacetimes, highlighting deviations from standard General Relativity. We analyze image formation and magnification for strong lensing, incorporating modified gravity effects into the lens equations. We calculate key parameters such as the angular radius of Einstein rings, the time delays and magnification ratios. Our findings indicate distinct observational signatures in modified gravity models, providing valuable insights for distinguishing these theories through gravitational lensing observations.

Chapter 1

Introduction

Historical Background

Albert Einstein first introduced the concept of gravitational lensing in the early 20th century [2], as part of the predictions arising from his 1915 publication on the General Theory of Relativity [3]. He demonstrated that large celestial bodies could bend the path of light passing near them due to the curvature of spacetime. This phenomenon was first quantitatively confirmed by British astronomer Arthur Eddington after his observation of a solar eclipse in 1919 [4,5]. Subsequently, Russian physicist Orest Chwolson independently highlighted that a massive object could bend the light from a more distant object, resulting in the appearance of multiple images of the latter [6].

In 1937, Fritz Zwicky calculated the transverse mass and discussed the importance of observation of gravitational lensing [7]. He was the one who first realized its huge cosmological implications. Resolution techniques in observational astronomy were nearly nonexistent when Zwicky did his work [8]. In 1963 Sjur Refsdal documented in great detail the properties of point mass gravitational lens and proposed that geometrical optics can be applied for gravitational lensing effects [9].

After that, all of the research on gravitational lensing was theoretical. However, Weymann verified that the two identical quasar spectra obtained by Walsh and Carswell were gravitationally lensed pictures of a single quasar, Q0957 + 561. The field of gravitational lensing took off after this first gravitational lens system was discovered in 1979 [10]. Numerous photographs of a source observed by gravitational lensing carry much information about the lens and the source [11, 12].

Following the initial detection of a double quasar as a gravitational lens in

1979, gravitational lensing has made remarkable progress [13]. Walsh, Weymann, and Carswell recognized a double quasar shown in figure 1.1 through the quasar spectra. They found that the twin quasar is a single quasar whose image is distorted due to the gravitational influence of a foreground galaxy situated closer to Earth along the same line of sight [14]. In the 1980s;

Figure 1.1: The double quasar, a fascinating astronomical phenomenon, reveals two closely aligned images of the same quasar due to gravitational lensing. Source: ESA/Hubble.

theoretical advances and new lens discoveries helped to lay the groundwork for future research. The 1990s showed awesome pictures of Einstein's rings shown in figure 1.2 and arcs through the Hubble Space Telescope which gave us a better understanding of how the universe is structured.

In April 2019, researchers announced the discovery of the M87 black hole. Event Horizon Telescope (EHT) captured this image and revealed that a bright ring of hot gas encircles the shadow of a black hole. This black hole is 6.5 billion times that of the Sun and its location is about 55 million light-years away in the galaxy Messier 87. The achievement confirmed the existence of black holes and transformed black hole research. It was a milestone in astrophysics. These observations employed a global interferometric array containing eight telescopes, which operated at a wavelength of 1.3 mm [15]. Since 2019, the EHT has continued to collect data by incorporating more array elements and doubling its recording bandwidth [16].
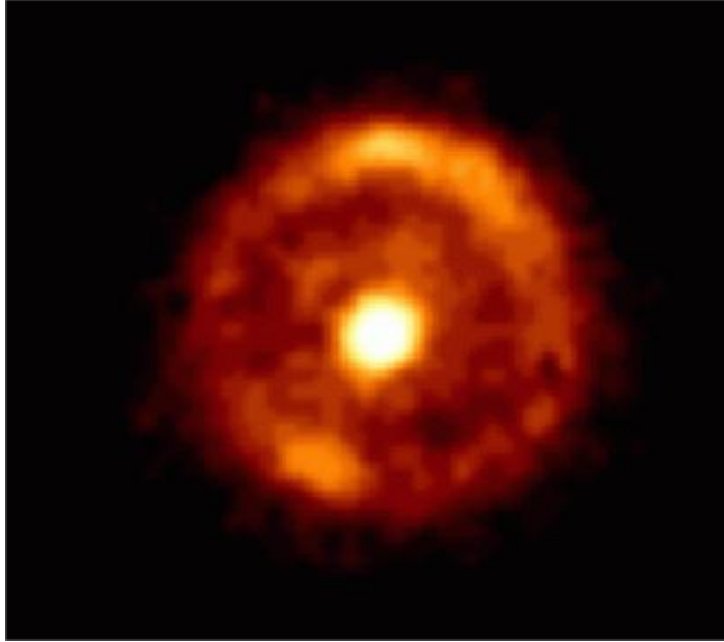
Figure 1.2: The Hubble Space Telescope captured an image of the distant galaxy 1938+666, which appears as an Einstein ring due to the gravitational lensing effect of a foreground galaxy. The intervening galaxy is visible as the bright spot at the center of the ring. This image was taken in the infrared spectrum, and the colors have been digitally assigned for clarity.

Motivation

In recent days, several challenges have been raised in gravitational lensing. New theories about the cosmic nature of galaxies have been developed. A modified theory of gravity was proposed to study the dark matter present in the universe. It aims to explain phenomena such as gravitational lensing. The theory suggests that some gravity interactions at the cosmic scales do not follow Einstein's predictions, lending a new way to explore the universe. For instance, a Schwarzschild-modified gravity (SMOG) black hole incorporates modifications due to alternative gravitational theories [17–20]. These solutions are important in probing the limits of general relativity, exploring quantum gravity, and understanding cosmological phenomena beyond Einstein's theory.

In 2015, the derivation of a regular singularity-free modified solution by using new linear field dynamics for the repulsive gravitational field components was done and renewable physical energy-momentum tensors were

discussed in modified gravity [21]. This approach prevents the formation of singularities, which are points where physical quantities like density and curvature become infinite. Later on, theoretical research on the shadow of rotating and non-rotating modified gravity black holes was conducted and found that shadow depends on parameters M and angular momentum J. In this research, different cases of shadow formation are discussed with distinct values of free parameter α [22].

In 2016, the analysis of thermodynamic properties of black holes in modified gravity was conducted, and it was proposed that without dark matter the correct rotation of galaxies and galaxy clusters can be studied through modified theory. In this research, it was shown that the Hawking temperature and evaporation profile of SMOG resembled a modified standard Schwarzschild black hole [23]. In the same year, the nature of gravitational waves is investigated in generalized gravitation theory known as MOG in literature. The study of the remarkable merger of two black holes, along with the detection of gravitational waves from LIGO events GW150914 and GW151226, was discussed in [24].

In 2018, the gravitational and electromagnetic perturbations of quasinormal modes were calculated in modified gravity also known as STVG spacetime. They have demonstrated the effect of increasing parameter α on the real and imaginary parts of quasinormal mode and compared the situation with the standard Schwarzschild case [25]. In 2021, the derivation of a regular rotating dark compact object was done in modified gravity and referred to as Schwarzschild modified gravity (SMOG) black hole. A rotating MOG dark compact object was also obtained in the same research. They form Schwarzschild black hole and Kerr black hole respectively, when a free parameter α is zero [26].

New activities for Schwarzschild-modified gravity black holes have produced interesting research in different fields [27, 28]. It has been shown that black hole solutions in a rotating universe are dual to the constant curvature $f(R)$ gravity theories and Einstein-Maxwell gravity, thus, revealing the power of black holes [29].

This thesis investigates the phenomena of strong and weak lensing in modified gravity spacetime [30]. The primary objective is to study the observable effects using M87* and Sgr A* as gravitational lenses within a static modified spacetime framework. Another concept of logarithmic distortion as in [31] will be explored in a static modified gravity black hole using the weak

deflection angle of light. The time delays for twenty-one different galaxies is also studied in modified gravity.

Now we will briefly explain some basic concepts related to the thesis topic. Throughout this dissertation, we have taken the value of gravitational constant G and the speed of light c as 1.

1.1 Metric Tensor

In the framework of GR, $g_{\mu\nu}$ is a symmetric and bi-linear form on the 4-dimensional Lorentzian manifold M. It describes the geometric and causal structures of spacetime. The metric tensor explains the curvature of spacetime caused by Riemannian curvature and determines the gravitational field. The metric tensor allows us to find the intervals between two events in spacetime. For any infinitesimal displacement, the interval ds^2 is defined as

$$ds^2 = g_{\mu\nu}dx^\mu dx^\nu, \qquad \mu, \nu = 0, 1, 2, 3. \qquad (1.1)$$

It is usually non-degenerate $g = \det(g_{\mu\nu}) \neq 0$. The components of the Einstein tensor such as Ricci scalar (R), and Ricci tensor (R_{ab}) can be defined through metric tensor. The Einstein tensor G_{ab} is defined as follows as

$$G_{\mu\nu} = R_{\mu\nu} - \frac{1}{2}g_{\mu\nu}R.$$

The Einstein tensor is used in Einstein's field equations to relate spacetime curvature to the energy and momentum of matter and radiation. The Einstein field equations are

$$G_{\mu\nu} = 8\pi T_{\mu\nu}, \qquad (1.2)$$

where $T_{\mu\nu}$ is the energy-momentum tensor. It describes the distribution and flow of energy and momentum in spacetime. The signature of the metric tensor describes the geometry of space. For example, in general relativity, the spacetime metric tensor has the signatures $(+, -, -, -)$ or $(-, +, +, +)$, which account for one-time and three spatial dimensions.

1.2 Geodesics

Geodesics is the generalization of straight lines to the curved space or spacetime. They represent the most direct path between two points in curved space, with a consistent tangent direction along the entire length of the curve. Let $x^\mu(\lambda)$ represent the worldline or trajectory, and $\frac{dx^\mu}{d\lambda}$ denote the tangent

vector field along $x^\mu(\lambda)$. The tangent vector is parallel-transported to the curve if the following condition is satisfied [32]

$$\frac{d^2x^\mu}{d\lambda^2} + \Gamma^\mu_{\nu\sigma}\frac{dx^\nu}{d\lambda}\frac{dx^\sigma}{d\lambda} = 0. \tag{1.3}$$

In flat spacetime, there is no curvature and the principles of Euclidean space are followed. The Minkowski spacetime denoted by $\eta_{\mu\nu}$ is used in the case of flat spacetime defined as

$$\eta_{\mu\nu} = \text{diag}(-1, +1, +1, +1).$$

The motion of freely falling objects is in a straight line when the spacetime is flat. The second derivative of x^μ is zero in this spacetime because the Christoffel symbols $\Gamma^\mu_{\nu\sigma}$ vanish (there is no curvature).

$$\frac{d^2x^\mu}{d\lambda^2} = 0. \tag{1.4}$$

Hence, the motion of the particle can be described through geodesics. The geodesics in spacetime can be classified into three types based on their properties and the nature of the paths they represent. Time-like geodesics correspond to the trajectories of particles and objects moving slower than the speed of light, describing how massive objects travel through spacetime. Null (light-like) geodesics represent the paths taken by light rays and other massless particles, illustrating the fastest possible travel at the speed of light. Space-like geodesics are theoretical paths requiring faster-than-light travel, which is physically impossible for any object or signal.

These distinctions help understand objects' movement and interaction within the framework of general relativity. We adopt the metric signatures $(-, +, +, +)$. Mathematically,

1. Space-like geodesics are characterized by a positive interval $(ds^2 > 0)$ in the spacetime metric.

2. Null geodesics are characterized by a zero interval ($ds^2 = 0$) in the spacetime metric.

3. Time-like geodesics are characterized by $(ds^2 < 0)$ in spacetime metric.

1.3 Impact Parameter

An impact parameter is a fundamental concept in gravitational lensing and relativistic phenomena. It is the shortest distance between the center of a massive body and the photon's path as it passes by as shown in figure 1.3. Due to the gravitational effects, it is considered a straight line. The value of an impact parameter, typically represented by b is calculated mathematically by expression [33]

$$b = \frac{\ell}{E}. \tag{1.5}$$

Here, E and ℓ are the energy and angular momentum of the upcoming photon[1] respectively. Understanding and accurately calculating the impact parameter is necessary for observing Einstein Rings, multiple image formation, and other lensing-related phenomena. A specific value of impact parameter called **critical impact parameter** is the specific value of the impact parameter for which the gravitational lensing effect causes the light from a background source to form an Einstein ring around the lensing object. The critical impact parameter predicts that either light will deflect or be captured by the black hole. Suppose that light has an impact parameter denoted by b and the critical impact parameter is represented by b_c, then

- If $b > b_c$, the light deflects and an image will form.

- If $b < b_c$, the light will be captured by a black hole and never deflect.

1.4 Effective Potential

In gravitational lensing, an effective potential is used to analyze the bending of light. It provides insight into the trajectory of light by integrating the gravitational attraction of the massive body with the centrifugal forces acting upon it. This concept is beneficial when analyzing the trajectories of light rays. The effective potential is related to the gravitational attraction and angular momentum barriers. Effective potentials (V_{eff}) are typically used to describe photon motion by combining kinetic and potential energy in curved spacetime. By using the norm of four-velocity u^μ as $u^\mu u_\mu = 0$, we obtain from the Lagrangian

$$\dot{r}^2 = E^2 - V_{\text{eff}}.$$

---

[1] An "upcoming photon" refers to a photon that is approaching a given point or observer in space, typically in the context of light propagation and detection.
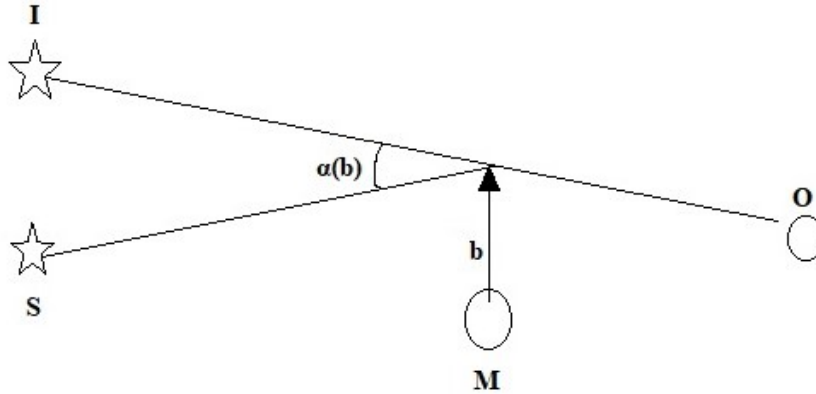
Figure 1.3: A sketch of a gravitational lens system showing the impact parameter, b, which represents the closest distance between the light ray's path and the center of the massive lensing body. The diagram includes the deflection angle, $\alpha(b)$, with O as the observer, S as the light source, M as the mass of the lensing body, and I as the image observed by the receiver.

The effective potential allows for the analysis of stable and unstable circular orbits. Mass M, energy E, and angular momentum ℓ help to define the effective potential. Circular orbits exist at turning point r_t, where $\dot{r} = 0$ and corresponds to the equation

$$\frac{dV_{\text{eff}}(r)}{dr}\bigg|_{r=r_t} = 0.$$

To determine whether circular orbits are stable or unstable, at the turning point r_t, find the second derivative of V_{eff} which corresponds to the radius of the circular orbits.

$$\frac{d^2V_{\text{eff}}}{dr^2}\bigg|_{r=r_t}.$$

The following cases will arise

- If $\frac{d^2V_{\text{eff}}}{dr^2}\bigg|_{r=r_t} > 0$, the orbit is stable which means that a small perturbation will tend the particle to move in original circular orbit. In this case, the effective potential near r_t has a local minimum.

8
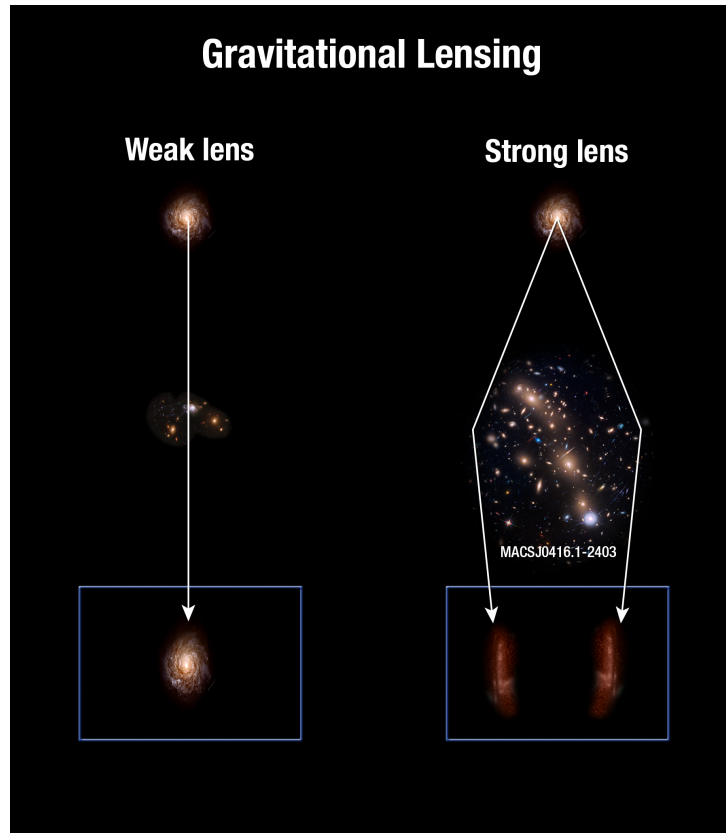
Figure 1.4: The phenomenon of weak lensing (left) and strong lensing (right) is shown here. Source: astrobites.org.

- If $\left.\frac{d^2 V_{\text{eff}}}{dr^2}\right|_{r=r_t} < 0$, the orbit is unstable which means that a small perturbation will tend the particle to move away from its original circular orbit. In this case, the effective potential near r_t has a local maximum.

1.5   Gravitational Lensing

Gravitational lensing is the phenomenon where light from a distant object, like a star or galaxy, bends around a massive object between the observer and the light source. This bending creates images of the distant object, which can be magnified or distorted depending on how close the light path comes to the massive object. This effect is explained by general relativity, which says that light travels along paths known as geodesics in spacetime. There are different types of gravitational lensing, which are described below.

1.5.1 Strong Gravitational Lensing

This occurs when the lensing object is large, resulting in notable light deflection. This can produce several images, arcs, or even whole rings (Einstein rings) of the background source 1.4. Strong lensing provides significant magnification and can be used to study the lensing mass and the background source in great detail.

1.5.2 Weak Gravitational Lensing

In weak lensing, the smaller deflection of light causes slight distortions in the shapes of background galaxies [33] as shown in figure 1.4. By statistically analyzing these small distortions across many galaxies, astronomers can investigate the distribution of dark matter throughout the cosmos. This method is one of the most successful approaches for mapping with dark matter which remains undetectable by conventional telescopes because it does not emit light. Astronomers can produce detailed maps of dark matter in galaxy clusters and large-scale structures by analyzing the lensing effects on background galaxies.

1.5.3 Microlensing

Microlensing happens when a small object, like a star or planet, passes before a larger star. The gravitational field of the foreground object behaves like a lens by bending and focusing the light coming from a background star as in figure 1.5. Unlike strong lensing, microlensing does not create numerous pictures but rather creates a brief rise in the brightness of the background star. Microlensing events are used to detect dark objects in the Milky Way, including exoplanets and black holes as well as to explore the distribution of invisible matter.

1.6 Gauss-Bonnet Theorem

The topology of any freely adjustable surface is explained through the Gauss-Bonnet theorem. It establishes a link between the overall Gaussian curvature of a surface and its Euler characteristic. While the theorem is commonly stated for compact, directed surfaces without boundaries, other versions exist for surfaces with boundaries [34].

Statement: A freely orientable surface described as a two-dimensional curved surface has Gaussian curvature K and a small area element ds. The surface is accompanied by various boundaries which are differentiable curves,
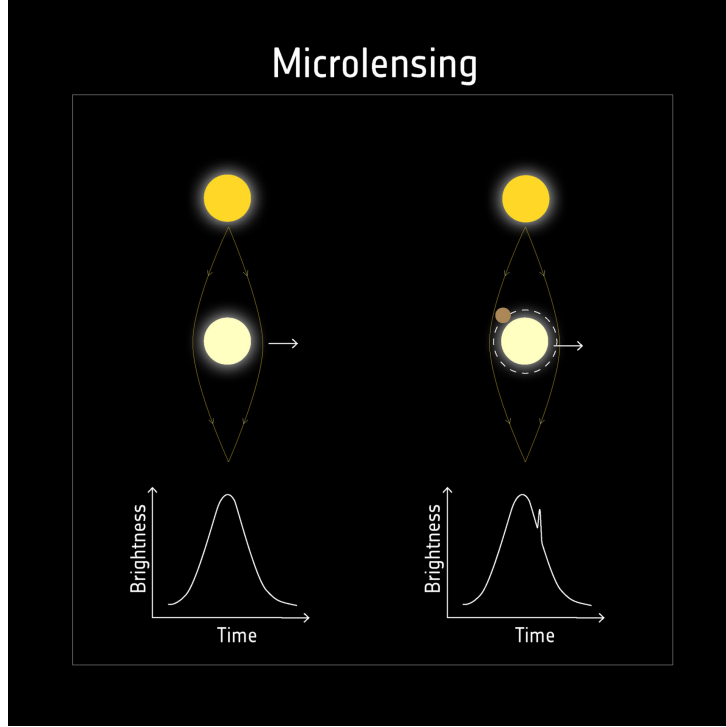
Figure 1.5: The phenomenon of microlensing is shown in the above figure. Source: European Space Agency.

denoted by ∂C_i, with geodesic curvature k_g. The angles along the vertices are taken as θ_i called jump angles shown in figure 1.6. Then the general form of Gauss-Bonnet theorem is [35–38]

$$\iint_D K dS + \sum_{i=1}^{N} \int_{\partial C_i} k_g dl + \sum_{i=1}^{N} \theta_i = 2\pi.$$

Here, the notation K is used for the Gaussian curvature of the surface and dS is the area element. Geodesic curvature is denoted by the term k_g which indicates how far the deviation of C_i occurs from the geodesics. If C_i is the geodesics then $k_g = 0$.

The Gaussian curvature K indicates the way a surface is curved. Its value can be calculated by following a mathematical formula [39]

$$K = -\frac{1}{\sqrt{\bar{g}_{rr}\,\bar{g}_{\phi\phi}}}\left[\frac{\partial}{\partial r}\left(\frac{1}{\sqrt{\bar{g}_{rr}}}\frac{\partial\sqrt{\bar{g}_{rr}}}{\partial r}\right) + \frac{\partial}{\partial\phi}\left(\frac{1}{\sqrt{\bar{g}_{\phi\phi}}}\frac{\partial\sqrt{\bar{g}_{rr}}}{\partial\phi}\right)\right].$$

The value of k_g along the geodesics C_i is calculated through the following
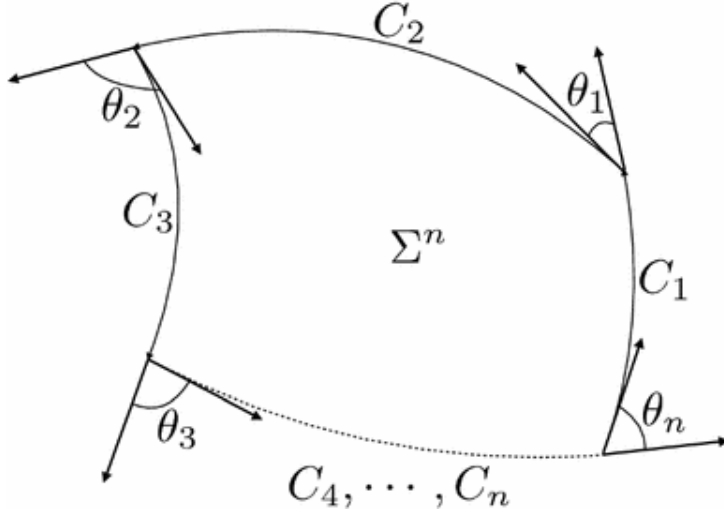
Figure 1.6: The schematic diagram of a surface having differentiable curves along with jump angles is represented here.

formula [40]

$$k_g = \frac{1}{2\sqrt{\bar{g}_{rr}\,\bar{g}_{\phi\phi}}} \left(\frac{\partial \bar{g}_{\phi\phi}}{\partial r} \frac{d\phi}{d\tilde{t}} - \frac{\partial \bar{g}_{rr}}{\partial \phi} \frac{dr}{d\tilde{t}} \right) + \frac{d\Phi}{d\tilde{t}}.$$

where Φ is the angle between the tangent vector of the curve and the radial unit vector.

1.7 Magnification, Lens Equation, and Einstein Rings

The ideas of magnification and lens equations get more difficult in general relativity due to spacetime curvature. The Lens equation in gravitational lensing relates the source position, the lens position, and the image position. Bozza analyzed various lens equations in [41]. At first, the lens equation in its most general form is [41]

$$\delta = \vartheta - \frac{D_{ls}}{D_s}\hat{\alpha}(\vartheta). \tag{1.6}$$

D_{ls} is the lens-source distance and D_s is the observer-source distance. δ and ϑ are the angular positions of the source and image, respectively shown in figure 1.7. Later on, Virbhadra and Ellis proposed a lens equation [42] which
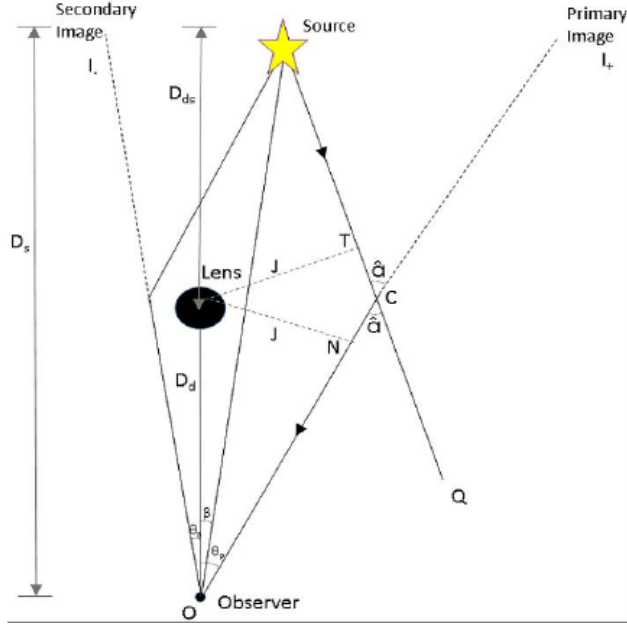
Figure 1.7: The gravitational lensing phenomenon is portrayed in which light comes from the source and is deflected by the lensing body.

is

$$\tan \delta = \tan \vartheta - \frac{\mathrm{D_{ls}}}{\mathrm{D_s}}[\tan \vartheta + \tan(\alpha - \vartheta)],$$

here, α is the angle of deflection of light. The traditional lens equation given earlier was suitable for the scenario of weak gravitational lensing. In contrast, the equation designed by Virbhadra and Ellis is useful for studying strong gravitational lensing effects.

Magnification in gravitational lensing is defined as the ratio of the image's solid angle to that of the source. The increase or decrease in size of an image as compared to the original form after lensing is seen through magnification. Its value is calculated from the Jacobian determinant [43]

$$\mu = \left| \det \frac{\partial \delta}{\partial \vartheta} \right|^{-1}.$$

The partial derivative of (1.6) gives

$$\frac{\partial \delta}{\partial \vartheta} = 1 - \frac{\mathrm{D_s}}{\mathrm{D_{ls}}} \left(\frac{\partial \hat{\alpha}}{\partial \vartheta} \right).$$

13
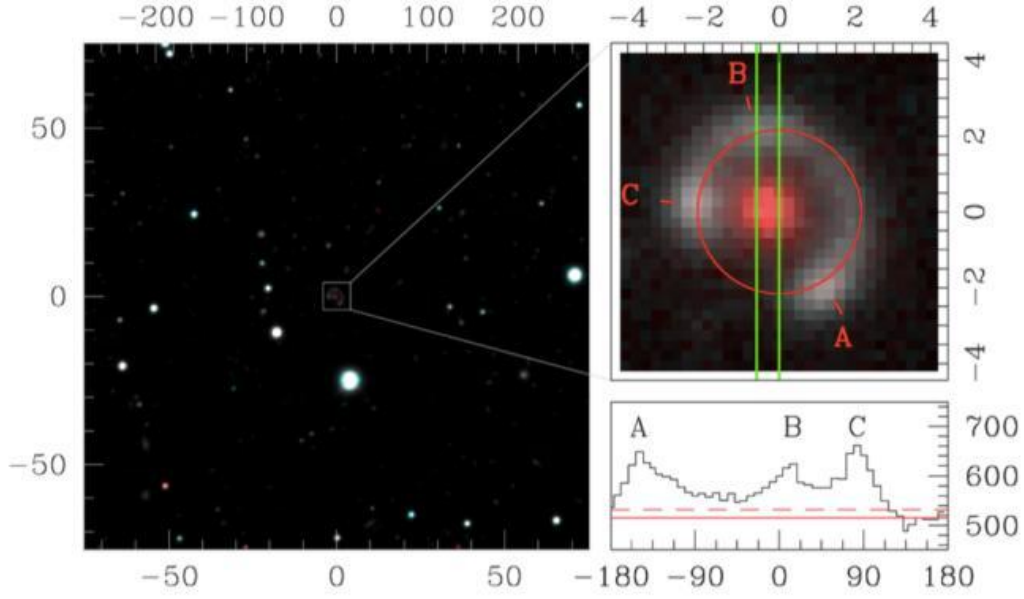
Figure 1.8: A newly discovered Einstein ring is shown here.

Substitution of above expression in μ, we get

$$\mu = \frac{1}{\left| 1 - \frac{D_s}{D_{ls}} \frac{d\vartheta}{d\alpha} \right|}. \tag{1.7}$$

but in the study of gravitational lensing, it is calculated by using the formula [44]

$$\mu = \mu_t \mu_r$$

where

$$\mu_t = \left(\frac{\sin\delta}{\sin\vartheta} \right)^{-1}, \qquad \text{and} \qquad \mu_r = \left(\frac{d\delta}{d\vartheta} \right)^{-1}.$$

There are two types of magnification: Radial magnification μ_r and Tangential magnification μ_t. Radial magnification occurs along the direction of the line connecting the lens and the source. It describes how the image is stretched or compressed radially towards or away from the lens. Tangential magnification occurs along the direction perpendicular to the line connecting the lens and the source. It describes how the image is stretched tangentially around the lens.

14

An Einstein ring occurs when the light from a distant background source, such as a galaxy or quasar, is deflected by a massive body like a galaxy or a galaxy cluster shown in figure 1.8. The foreground object's gravitational field functions as a lens, bending the light from the background source into a ring shape around the lensing object. The backdrop source, lensing object, and observer must all be aligned along the same line of sight to form an Einstein ring. For an Einstein ring to be visible, an observer, lens, and source must be aligned. The angular radius of the Einstein ring θ_E is provided by [45]:

$$\theta_E = \sqrt{\frac{4GM}{c^2} \frac{D_{ls}}{D_{ol}D_s}},$$ (1.8)

where M is the mass of the massive body, and c is the speed of light. These principles are essential for a thorough understanding of gravitational lensing.

Chapter 2

Review: Analyzing Gravitational Lensing Patterns Around Strongly Null Naked Singularities

This chapter presents a comprehensive review of the article mentioned above [46]. The main purpose of this chapter is to analyze and study the gravitational lensing method in strong gravity. The article covers the expression of deflection angle and then a few observations. The mathematical expressions and observations are then compared to the Schwarzschild spacetime to investigate the difference between a black hole and a naked singularity.

An event horizon(boundary beyond which nothing can escape even light) is absent in naked Singularity spacetime. This singularity can be seen through the naked eye. According to cosmic censorship conjecture, there is no naked singularity [47]. It was proposed by Penrose in 1965. In a strongly null naked singularity there is no photon sphere and the event horizon [46].

Joshi and collaborators proposed this strongly null naked singularity in [48] and also studied the shadow of this spacetime. In [46], Suvankar Paul calculated the deflection angle of naked singularity in strong gravity.

We have structured this chapter in the following way. In Section 2.1, we have provided a brief overview of light trajectories and effective potential. This section serves as a foundation for the next discussions. Section 2.2 is about calculating the deflection angle and includes a few observations about the images formed after deflection. In addition, we include plots to understand the behavior and characteristics of light around a naked singularity in detail. Section 2.3 discusses a few situations involving the bending angle of distinct spacetimes to build a thorough knowledge of the concept.

The line element of naked singularity which is static (non-rotating) and spherically symmetric is given as [46]

$$ds^2 = -\frac{dt^2}{\left(1+\frac{M}{r}\right)^2} + \left(1+\frac{M}{r}\right)^2 dr^2 + r^2 d\Omega^2. \qquad (2.1)$$

Here, $d\Omega^2 = dr^2 + \sin^2\theta d\phi^2$. In the limit, $r \to \infty$, this line element given in (2.1) reduces to Minkowski spacetime which is flat. This suggests that (2.1) is asymptotically flat. Expansion of g_{rr} is

$$g_{rr} = \left(1+\frac{M}{r}\right)^2 = \frac{1}{\left(1+\frac{M}{r}\right)^{-2}} = \frac{1}{\left[1 - \frac{2M}{r} + \frac{3M}{r^2} - \cdots\right]}. \qquad (2.2)$$

There is no event horizon in this spacetime which can be seen through the expansion of g_{rr} having a positive and finite solution for $r > 0$. Hence, a globally naked singularity exists in the given spacetime. This naked singularity will resemble a Schwarzschild black hole for large values of r. The reason for the similarity is the radius of the Einstein ring which is almost sane for both spacetimes.

2.1 Characteristics of Null Geodesics

The Lagrangian for the given spacetime is

$$\mathcal{L} = \frac{m}{2} g_{ab} \dot{x}^a \dot{x}^b = \frac{m}{2} \left[-\frac{1}{\left(1+\frac{M}{r}\right)^2} \dot{t}^2 + \dot{r}^2 \left(1+\frac{M}{r}\right)^2 + r^2 \dot{\vartheta}^2 + r^2 \sin^2\vartheta \dot{\phi}^2 \right]. \qquad (2.3)$$

In this dissertation, the $\dot{}$ symbolizes the derivative with respect to the geodetic parameter λ. We will consider the nature of null geodesics ($ds^2 = 0$). We can take $\vartheta = \frac{\pi}{2}$ without losing generality because spacetime is spherically symmetric. The Lagrangian reduces to

$$\mathcal{L} = \frac{m}{2} \left[\left(1+\frac{M}{r}\right)^2 \dot{r}^2 - \frac{\dot{t}^2}{\left(1+\frac{M}{r}\right)^2} + r^2 \dot{\phi}^2 \right]. \qquad (2.4)$$

Further, this spacetime is static and spherically symmetric so E and angular momentum ℓ will be conserved. The corresponding value of $\dot{t}$ and $\dot{\phi}$ will be calculated by using the Euler Lagrange equation defined as

$$\frac{d}{d\lambda}\left(\frac{\partial \mathcal{L}}{\partial \dot{x}^\nu}\right) = \left(\frac{\partial \mathcal{L}}{\partial x^\nu}\right). \qquad (2.5)$$

When $\nu = 0$, (2.3) and (2.5) give

$$\dot{t} = E\left(1 + \frac{M}{r}\right)^2.$$ (2.6)

Similarly, when $\nu = 3$ in (2.5), we obtain

$$\dot{\phi} = \frac{\ell}{r^2}.$$ (2.7)

Using null geodesics condition ($ds^2 = 0$), we obtain

$$\left(1 + \frac{M}{r}\right)^2 \dot{r}^2 - \frac{\dot{t}^2}{\left(1 + \frac{M}{r}\right)^2} + r^2\dot{\phi}^2 = 0.$$

Substituting $\dot{t}$ and $\dot{\phi}$ in above equation yields

$$\dot{r}^2 = E^2 - \frac{\ell^2}{r^2(1 + \frac{M}{r})^2},$$ (2.8)

where $V_{\text{eff}} = \frac{\ell^2}{r^2(1+\frac{M}{r})^2}$ is the effective potential of the particle. The effective potential has no extremum as shown in figure 2.1, so it does not possess a photon sphere. At the turning point of the light r_t, we have $\dot{r} = 0$ which gives

$$V_{\text{eff}} = \frac{\ell^2}{(r_t + M)^2}.$$ (2.9)

The impact parameter is the shortest distance measured perpendicularly from the source to the lensing body. The smaller impact parameter results in a greater bending of the light. Mathematically, the impact parameter at the turning point is defined as

$$b(r_t) = \frac{\ell}{E} = r_t + M.$$ (2.10)

2.2   Bending of light in the SDL

The deflection of light forming an angle will be studied in this section. Now, a spacetime having a photon sphere has a unique property. The angle diverges due to the presence of a photon sphere. The reason is the rotation of light rays around the lensing body before moving back toward the observer. The formation of shadow in the given spacetime does not depend on the photon
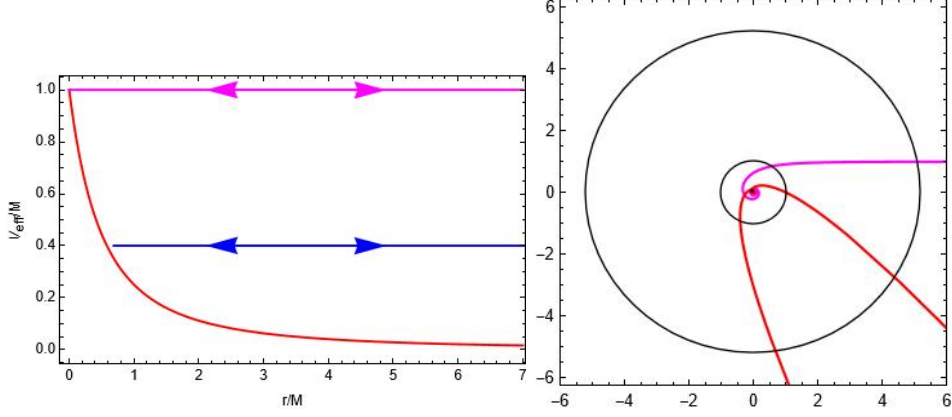
Figure 2.1: The V_{eff} is plotted against r/M in the left figure. The corresponding light trajectories are shown in the right figure. The black circle represents the shadow edge of naked singularity spacetime.

The pink and blue lines are the light trajectories having $b < b_c$ and $b > b_c$ respectively. On the right side, the corresponding light trajectories are plotted in which a pink light ray is captured into a massive body, and a red one is deflected back. The big circle shows the Schwarzschild shadow region and the smaller one is for naked singularity.

sphere. It will be interesting to figure out the cause which forms a shadow here. Rearrangement of (2.8) gives us

$$\dot{r} = \pm\sqrt{E^2 - \frac{\ell^2}{r^2(1 + \frac{M}{r^2})^2}}. \tag{2.11}$$

To calculate the angle of bending of light, we will find the expression of $\frac{d\phi}{dr}$ by combining the above expression with (2.7),

$$\begin{aligned}
\frac{d\phi}{dr} &= \frac{\dot{\phi}}{\dot{r}}, \\
&= \pm\frac{\ell}{r^2\sqrt{E^2 - \frac{\ell^2}{(r+M)^2}}}, \\
\frac{d\phi}{dr} &= \pm\frac{b}{r^2\sqrt{1 - \frac{b^2}{(r+M)^2}}}.
\end{aligned} \tag{2.12}$$

By using $b(r_t) = r_t + M$, above equation can be rewritten as

$$\frac{d\phi}{dr} = \pm\frac{(r_t + M)(r + M)}{r^2\sqrt{r^2 + 2(r - r_t)M - r_t^2}}. \tag{2.13}$$

19
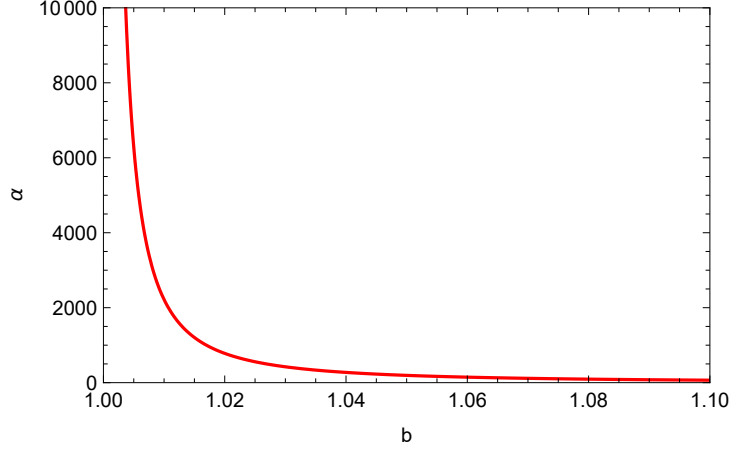
Figure 2.2: Bending angle α is plotted for different values of b.

Integration of the above expression will give us

$$\phi(r) = \phi(\infty) \pm \int_r^\infty \frac{(r_t + M)(r + M)}{r^2\sqrt{r^2 + 2(r - r_t)M - r_t^2}} dr. \qquad (2.14)$$

The initial azimuthal angle is given by ϕ_∞, generated by the light ray from the source in the asymptotic area. As a result, the gravitational field generated by the naked singularity bends light with an expression

$$\alpha(r_t) = 2|\phi(r_t) - \phi_\infty| - \pi,$$
$$\alpha(r_t) = \int_{r_t}^\infty \frac{(r_t + M)(r + M)}{r^2\sqrt{r^2 + 2(r - r_t)M - r_t^2}} dr - \pi. \qquad (2.15)$$

The analytic expression of α is obtained through some simplification steps

$$\alpha(r_t) = \frac{2M(r_t + M)}{r_t(r_t + 2M)} + \frac{4(r_t + M)^3}{r_t^{3/2}(r_t + 2M)^{3/2}} \arctan\sqrt{\frac{r_t}{r_t + 2M}} - \pi.$$

Using the property $\arctan(\frac{1}{a}) = \frac{\pi}{2} - \arctan a$, in the above expression results in

$$\alpha(r_t) = \frac{2M(r_t + M)}{r_t(r_t + 2M)} + \frac{4(r_t + M)^3}{r_t^{3/2}(r_t + 2M)^{3/2}} \arctan\sqrt{1 + \frac{2M}{r_t}} - \pi. \qquad (2.16)$$

By using the value of the impact parameter, the above expression reduces to the form

$$\alpha(b) = \frac{2Mb}{b^2 - M^2} + \frac{4b^3}{(b^2 - M^2)^{3/2}} \arctan\sqrt{\frac{b + M}{b - M}} - \pi. \qquad (2.17)$$

20

From (2.16) and (2.17), one can easily see that the divergence of deflection angle occurs when the impact parameter reaches the critical impact parameter $b \to b_c = M$ or equivalently, $r_t \to 0$. Expansion of α in the limit $x > 1$ is as

$$\alpha(r_t) = \frac{2\pi(r_t + M)^3}{r_t^{3/2}(r_t + 2M)^{3/2}} - \frac{2(r_t + M)(2r_t + 3M)}{(r_t + 2M)^2} + \frac{4(r_t + M)^3}{3(r_t + 2M)^3}$$
$$- \frac{4r_t(r_t + M)^3}{5(r_t + M)^4} + \cdots - \pi,$$

and

$$\alpha(b) = \frac{2\pi(b/M)^3}{\frac{b^2}{M^2} - 1} - \frac{2(b/M)(\frac{2b}{M} + 1)}{(\frac{b}{M} + 1)^2} + \frac{4(b/M)^3}{3(b/M + 1)^3} - \frac{4(b/M)^3(\frac{b^2}{M^2} - 1)}{(\frac{b}{M} + 1)^5} + \cdots - \pi.$$

(2.18)

Hence, after divergence of $\alpha(r_t)$ in the limit $r_t \to 0$ and $b \to b_c = M$ (2.18) takes the form

$$\lim_{b \to b_c} \alpha(b) = \left[\frac{2\pi(b/M)^{3/2}}{\left(\frac{b^2}{b_c^2} - 1\right)^{3/2} 2^{3/2}} - \frac{2(b_c/M)(\frac{2b_c}{M} + 1)}{\left(\frac{b_c}{M} + 1\right)^2} + \cdots \right] - \pi,$$

$$= \left[\frac{2\pi(b/M)^{3/2}}{\left(\frac{b^2}{b_c^2} - 1\right)^{3/2} 2^{3/2}} - \frac{6}{4} + \frac{1}{6} - 0 + \cdots \right] - \pi.$$

If we simplify and ignore higher-order terms then it will yield

$$\lim_{r_t \to 0} \alpha(r_t) = \frac{\pi}{\sqrt{2}} \left(\frac{M}{r_t}\right)^{3/2} - \frac{4}{3} - \pi + O(r_t),$$

$$\lim_{b \to 0} \alpha(b) = \frac{\pi/\sqrt{2}}{\left(\frac{b}{b_c} - 1\right)^{3/2}} \left(\frac{M}{r_t}\right)^{3/2} - \frac{4}{3} - \pi + O\left(\frac{b}{b_c} - 1\right).$$

(2.19)

The formula above is classified as a non-logarithmic polynomial divergence as $b \to b_c$ and $r_t \to 0$. This behavior is a distinctive characteristic of a naked singularity.

2.3 Methods to Calculate Bending Angle

We will discuss different cases to understand the procedure to find the bending angle in two distinct spacetimes.

2.3.1 Strong deflection angle of spacetime having a photon sphere only

Now we will only study the deflection angle of a spacetime with a photon sphere. For this spacetime, the bending angle diverges in the limit $b \to b_c$ and $r_t \to 0$ as light approaches from the $b > b_c$ side. Logarithmic divergence exists for this spacetime. Bozza [49] initially researched this, then Tsukumoto [50] refined it. Suppose a static, spherically symmetric, and asymptotically flat spacetime to study the strong deflection angle. The metric tensor for the following spacetime is given as

$$ds^2 = -A(r)dt^2 + B(r)dr^2 + C(r)(d\theta^2 + \sin^2\theta d\phi^2), \qquad (2.20)$$

where $A(r)$, $B(r)$ and $C(r)$ satisfies

$$
\begin{aligned}
\lim_{r\to\infty} A(r) &= 1, \\
\lim_{r\to\infty} B(r) &= 1, \\
\lim_{r\to\infty} \frac{C(r)}{r^2} &= 1,
\end{aligned}
\qquad (2.21)
$$

which is the condition for asymptotic flatness. The static and spherically symmetric nature of the spacetime leads to conserved quantities namely energy and angular momentum. Also, we will find out a positive solution by putting $D(r) = 0$ and $D(r)$ is defined as

$$D(r) = \frac{C'}{C} - \frac{A'}{A}. \qquad (2.22)$$

The prime ($'$) represents the differentiation of the radial coordinate r. $D(r) = 0$ yields the photon sphere radius, r_{ph}. The path of light is represented by $g_{ab}k^a k^b$, where $k^a = \dot{x}^a$ represents the number of light waves. The dot ($\dot{}$) represents differentiation concerning the affine parameter, which parameterizes the light's trajectory. The conserved quantities include energy and angular momentum defined as

$$
\begin{aligned}
E &= A(r)\dot{t}, \\
\ell &= C(r)\dot{\phi}.
\end{aligned}
\qquad (2.23)
$$

The value of E and L are non-vanishing at the same time, so the impact parameter is defined as

$$b = \frac{\ell}{E} = \frac{C(r)\dot{\phi}}{A(r)\dot{t}}; \qquad\qquad E \neq 0. \qquad (2.24)$$

We will take $\theta = \frac{\pi}{2}$ without any loss of generality because the spacetime is static and spherically symmetric. The path of light coming from the source can be explained by an equation of trajectory given as

$$-A(r)\dot{t}^2 + B(r)\dot{r}^2 + C(r)\dot{\phi}^2 = 0. \tag{2.25}$$

After a few simplifications, we obtain

$$\dot{r}^2 = V(r),$$

where

$$V(r) \equiv \frac{L^2 R(r)}{B(r)C(r)},$$

and

$$R(r) = \frac{C(r)}{A(r)b^2} - 1.$$

Photon will orbit around the lensing body when $V(r) \geq 0$. This is because when the effective potential is negative and zero, the photon will not have enough energy to form a stable orbit. So, it will escape to infinity or fall into the central object. When we use the condition described in (2.21) for asymptotic flatness, we get $\lim_{r \to \infty} V(r) = E^2 > 0$, so the presence of photon at infinity can be expected. We assume that $R(r) = 0$ has one positive solution. Suppose the light ray coming nearer from infinity towards the lensing object will scatter at the closest distance $r = r_t$ and then go to infinity. There are some observations related to the nearest approach distance r_t:

- For the scattering case, $r_{ph} < r_t$ is satisfied, light does not reach the photon sphere. If $r_{ph} > r_t$, the photon will be captured by the lensing body's gravitational field, either orbiting around the photon sphere or falling into the massive object.

- $r = r_t$ is the largest solution of $R(r) = 0$. This is because the photon comes from infinity, and reaches r_t, and then moves away again.

- $B(r)$ and $C(r)$ do not diverge for $r \geq r_t$. Hence, $V(r)$ vanishes at $r = r_t$.

Since, $\dot{r} = 0$ at r_t, so (2.25) changes as

$$A_t \dot{t}_t^2 = C_t \dot{\phi}_t^2. \tag{2.26}$$

Throughout the discussion, subscript t denotes the quantities at $r = r_t$. By using (2.26), the impact parameter is defined as

$$b(r_t) = \frac{\ell}{E} = \sqrt{\frac{C_t}{A_t}}. \tag{2.27}$$

Using (2.27), we will rewrite $R(r)$ as

$$R(r) = \frac{A_t C}{A C_t} - 1.$$

The critical impact parameter is defined as [51]

$$b_c \equiv \lim_{r_t \to r_{ph}} \sqrt{\frac{C_t}{A_t}},$$

and $r_t \to r_{ph}$ and $b_t \to b_{ph}$ is referred as strong deflection limit. The trajectory of a light ray is rewritten as

$$\left(\frac{dr}{d\phi}\right)^2 = \frac{R(r)C(r)}{B(r)}, \tag{2.28}$$

and the deflection angle of light $\alpha(r_t)$ is obtained as

$$\alpha(r_t) = I(r_t) - \pi, \tag{2.29}$$

where $I(r_t)$ is defined as

$$I(r_t) \equiv \int_{r_t}^{\infty} \frac{dr}{\sqrt{\frac{R(r)C(r)}{B(r)}}}. \tag{2.30}$$

For simplification, introducing a new variable

$$z = 1 - \frac{r_t}{r}, \tag{2.31}$$

The term $I(r_t)$ is defined by

$$I(r_t) = \int_0^1 S(z, r_t) dz, \tag{2.32}$$

where $S(z, r_t)$ is defined as

$$S(z, r_t) \equiv \frac{2r_t}{\sqrt{F(z, r_t)}},$$
$$F(z, r_t) = \frac{RC}{B}(1 - z)^4. \tag{2.33}$$

Using the Taylor series expansion of $S(z, r_t)$ in powers of z as

$$S = S_t + S_t' r_t z + \left(\frac{1}{2} S_t'' r_t^2 + S_t' r_t\right) z^2 + O(z^3). \tag{2.34}$$

here, $'$ denotes derivative with respect to r. The first and second derivative of $R(r)$ is

$$R'(r) = \frac{A_t C'}{AC_t} - \frac{ACA'}{A^2 C_t},$$

$$R''(r) = \frac{C''_t}{C_t} - \frac{A''_t}{A} - 2\frac{C'_t A'_t}{A_t C_t} - \frac{2A'^2}{A_t^2},$$

By using (2.34), $R(r)$ can be expanded in the powers of z as

$$R(r) = \mathrm{D}_t r_t z + \frac{r_t}{2}\left[\left(\frac{C''_t}{C_t} - \frac{A''_t}{A_t}\right) + \left(1 - \frac{A'_t r_t}{A_t}\right)\mathrm{D}_t\right] r_t z^2 + O(z^3). \quad (2.35)$$

Now, we will expand $F(z, r_t)$ in power of z as follows

$$F'_t(z, r_t) = (1 - 4z + 6z^2)\left(\frac{\mathrm{D}_t C_t}{B_t}\right) + O(z^3),$$

$$F''_t(z, r_t) = (1 - 4z)\left(\frac{R''_t C_t}{B_t} + \frac{C'_t R'_t}{B_t} - \frac{B'_t R'_t C_t}{B_t^2} + \frac{C_t R'_t}{B_t} - \frac{R'_t C_t B'_t}{B_t^2}\right).$$

Using the above values and (2.34), we get

$$F(z, r_t) = \frac{RC}{B}(1 - 4z + 6z^2) + (1 - 4z)\left(\frac{\mathrm{D}_t C_t}{B_t}\right) r_t z$$

$$+ \left[\frac{1}{2}\left(\frac{R''_t C_t}{B_t} + \frac{C'_t R'_t}{B_t} - \frac{B'_t R'_t C_t}{B_t^2} + \frac{C_t R'_t}{B_t} - \frac{R'_t C_t B'_t}{B_t^2}\right) r_t^2 + \left(\frac{\mathrm{D}_t C_t}{B_t}\right) r_t\right] z^2$$

$$+ O(z^3).$$

Using the value of $R'(r_t)$, $R''(r_t)$ in the above expression, we obtain

$$F(z, r_t) = \frac{\left(\mathrm{D}_t r_t z + \frac{r_t}{2}\left[\left(\frac{C''_t}{C_t} - \frac{A''_t}{A_t}\right) + \left(1 - \frac{A'_t r_t}{A_t}\right)\mathrm{D}_t\right] r_t z^2\right) C}{B}(1 - 4z + 6z^2)$$

$$+ (1 - 4z)\left(\frac{\mathrm{D}_t C_t}{B_t}\right) r_t z$$

$$+ \left[\frac{1}{2}\left(\frac{C_t\left(\frac{C''_t}{C_t} - \frac{A''_t}{A_t} - 2\frac{C'_t A'_t}{A_t C_t} - \frac{2A'^2}{A_t^2}\right)}{B_t}\right.\right.$$

$$\left.+ \left(\frac{A_t C'}{AC_t} - \frac{ACA'}{A^2 C_t}\right)\left(\frac{C'_t}{B_t} - \frac{B'_t C_t}{B_t^2} + \frac{C_t}{B_t} - \frac{C_t B'_t}{B_t^2}\right)\right) r_t^2 + \left(\frac{\mathrm{D}_t C_t}{B_t}\right) r_t\right] z^2$$

$$+ O(z^3).$$

After a few simplifications and rearrangements, we can write $F(z, r_t)$ in the following form

$$F(z, r_t) = \sum_{n=1}^{\infty} c_n(r_t) z^n, \tag{2.36}$$

where $c_1(r_t)$ and $c_2(r_t)$ are given by

$$c_1(r_t) = \frac{C_t D_t r_t}{B_t}, \tag{2.37}$$

and,

$$c_2(r_t) = \frac{C_t r_t}{B_t} \left[D_t \left(\left(D_t - \frac{B_t'}{B_t} \right) r_t - 3 \right) + \frac{r_t}{2} \left(\frac{C_t''}{C_t} - \frac{A_t''}{A_t} \right) \right], \tag{2.38}$$

respectively. From the strong deflection limit $r_t \to r_{ph}$, the value of $D_{ph} = 0$ and

$$c_1(r_{ph}) = 0, \tag{2.39}$$

and

$$c_2(r_{ph}) = \frac{C_{ph} r_{ph}^2}{2 B_{ph}} D_{ph}', \tag{2.40}$$

where

$$D_{ph}' = \frac{C_{ph}''}{C_{ph}} - \frac{A_{ph}''}{A_{ph}}. \tag{2.41}$$

Now, the value of $F(z, r_{ph})$ reduces to

$$F(z, r_{ph}) = c_2(r_{ph}) z^2 + O(z^3). \tag{2.42}$$

The divergence of $F(z, r_{ph})$ exhibits a logarithmic nature in the strong deflection limit as r_t approaches r_{ph}. The leading term in the divergence behaves as z^{-1}. We express the integral $I(r_t)$ as the sum of a divergent part, $I_D(r_t)$, and a regular part, $I_R(r_t)$. The divergent part $I_D(r_t)$ is defined as

$$I_D(r_t) \equiv \int_0^1 S_D(z, r_t) dz, \tag{2.43}$$

and,

$$S_D(z, r_t) \equiv \frac{2 r_t}{\sqrt{c_1(r_t) z + c_2(r_t) z^2}}.$$

Evaluation of $I_D(r_t)$ will give

$$I_D(r_t) = \frac{4 r_t}{\sqrt{c_2(r_t)}} \log \frac{\sqrt{c_2(r_t)} + \sqrt{c_1(r_t) + c_2(r_t)}}{\sqrt{c_1(r_t)}}. \tag{2.44}$$

26

To obtain the required expression of the deflection angle in strong gravity, we expand $c_1(r_t)$ and $b(r_t)$ in the powers of $r_t - r_{ph}$ as follows

$$c_1(r_t) = \frac{C_{ph}r_{ph}D'_{ph}}{B_{ph}}(r_t - r_{ph}) + O(r_t - r_{ph})^2,$$

$$b(r_t) = b_c(r_{ph}) + \frac{1}{4}\sqrt{\frac{C_{ph}}{A_{ph}}}D'_{ph}(r_t - r_{ph})^2 + O(r_t - r_{ph})^3,$$

(2.45)

respectively. Further

$$b(r_t) - b(r_{ph}) = \frac{1}{4}\sqrt{\frac{C_{ph}}{A_{ph}}}D'_{ph}(r_t - r_{ph})^2,$$

$$(r_t - r_{ph}) = 2\sqrt{\frac{1}{D'_{ph}}}\left(\frac{b}{b_c} - 1\right)^{1/2}.$$

Using the expression of $r_t - r_{ph}$ obtained from $b(r_t)$ in $c_1(r_t)$ we obtain

$$\lim_{r_t \to r_{ph}} c_1(r_t) = \lim_{b \to b_c} \frac{2C_{ph}r_{ph}\sqrt{D'_{ph}}}{B_{ph}}\left(\frac{b}{b_c} - 1\right)^{1/2}.$$

(2.46)

Hence, the expression of $I_D(r_t)$ in the strong deflection limit is

$$I_D(r_t) = -\frac{r_{ph}}{\sqrt{c_2(r_{ph})}}\log\left(\frac{b}{b_c} - 1\right) + \frac{r_{ph}}{\sqrt{c_2(r_{ph})}}\log r_{ph}^2 D'_{ph}$$
$$+ O((b - b_c)\log(b - b_c)).$$

(2.47)

The regular part I_R is defined as

$$I_R(r_t) \equiv \int_0^1 S_R(z, r_t)dz,$$

(2.48)

where $S(z, r_t)$ is defined as

$$S_R(z, r_t) = S(z, r_t) - S_D(z, r_t).$$

To evaluate I_R in the strong deflection limit as r_t approaches r_{ph} or b approaches b_c, we expand $I(r_t)$ in powers of $r_t - r_{ph}$ and focus on the leading term $I_R(r_{ph})$. We then integrate the regular part both numerically and analytically.

$$I_R(r_t) = \int_0^1 S_R(z, r_{ph})dz + O((r_t - r_{ph})\log(r_t - r_{ph})),$$

$$I_R(b) = \int_0^1 S_R(z, b_c)dz + O((b - b_c)\log(b - b_c)).$$

(2.49)

In the strong zone of gravity, the deflection angle is defined as

$$\alpha = -\overline{a}\log\left(\frac{b}{b_c} - 1\right) + \overline{b} + O((b - b_c)\log(b - b_c)), \qquad (2.50)$$

where $\overline{a}$ and $\overline{b}$ is given as

$$\overline{a} = \sqrt{\frac{2B_{ph}A_{ph}}{C_{ph}''A_{ph} - A_{ph}''C_{ph}}},$$

$$\overline{b} = \overline{a}\log\left[r_{ph}^2\left(\frac{C_{ph}''}{C_{ph}} - \frac{A_{ph}''}{A_{ph}}\right)\right] + I_R(r_{ph}) - \pi, \qquad (2.51)$$

respectively. The above analysis can assist in finding the deflection angles of spacetime that are static, spherically symmetric, and asymptotically flat.

2.3.2 Bending angle from ultra-compact objects

According to the analysis by Bozza and Tsukamoto, light bends outside the photon sphere, meaning its turning point forms at that location. The SDL is calculated as the turning point approaches the radius of the photon sphere. However, this calculation is not suitable for examining photons that are reflected within the photon sphere. In such cases, it is necessary to consider the turning point of a photon to determine the positions of relativistic images. In [52], the author presents an analytical method to calculate the deflection angle of photons that are deflected inside the photon sphere. The region inside the photon sphere, where light is deflected, is referred to as the "antiphoton sphere," as illustrated in figure 2.3. Its radius is determined by finding the minimum point of the effective potential.

Consider a static, spherically symmetric spacetime having the line element

$$ds^2 = -A(r)dt^2 + B(r)dr^2 + C(r)(d\theta^2 + \sin^2\theta d\phi^2), \qquad (2.52)$$

where $A(r)$, $B(r)$, and $C(r)$ satisfy the asymptotic flatness condition described in (2.21). Here, $\theta = \pi/2$ is assumed for simplicity. The Lagrangian for this spacetime is expressed as

$$2\mathcal{L} = -A(r)\dot{t}^2 + B(r)\dot{r}^2 + C(r)\dot{\phi}^2. \qquad (2.53)$$

where an over-dot represents the derivative concerning the affine parameter. Since the spacetime is static and spherically symmetric, it admits two constants of motion: energy and angular momentum. By using Euler Lagrange
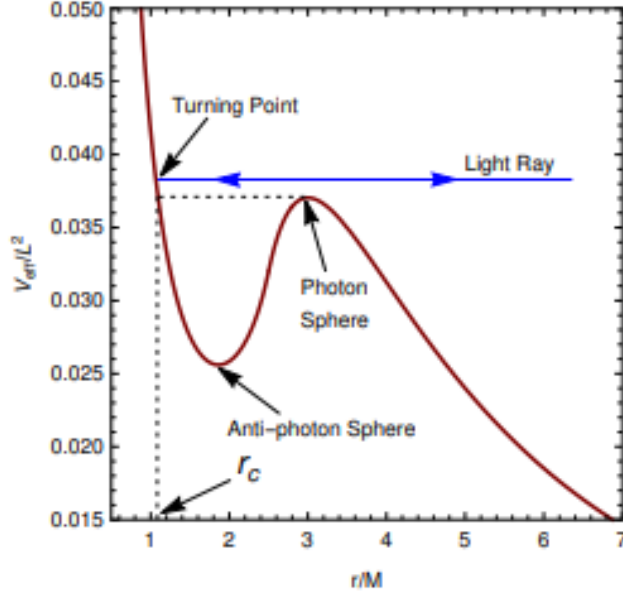
Figure 2.3: The effective potential of this spacetime is plotted. Here, r_c has the same radius as the turning point r_t.

equation, we obtain

$$\rho_t = \frac{\partial \mathcal{L}}{\partial \dot{t}} = -A(r)\dot{t} = -E, \qquad \rho_\phi = \frac{\partial \mathcal{L}}{\partial \dot{\phi}} = C(r)\dot{\phi} = \ell. \tag{2.54}$$

Using the null geodesics condition $g_{ab}\dot{x}^a\dot{x}^b = 0$, we find

$$AB\dot{r}^2 + V_{\text{eff}} = E^2, \qquad V_{\text{eff}} = \ell^2 \frac{A(r)}{C(r)}, \tag{2.55}$$

where V_{eff} is the effective potential. A photon coming from the source will turn at some radius r_t before reaching a faraway observer. At r_t, the condition $\dot{r} = 0$ holds. The impact parameter, calculated using this condition, is given by

$$b^2 = \frac{C(r_t)}{A(r_t)}. \tag{2.56}$$

The light is deflected by a massive body toward the faraway observer, resulting in a deflection angle

$$\alpha(r_t) = I(r_t) - \pi, \tag{2.57}$$

29

where

$$I(r_t) = 2 \int_{r_t}^{\infty} \frac{dr}{\sqrt{\frac{R(r)C(r)}{B(r)}}}, \qquad R(r) = \left(\frac{A_t C}{C_t A} - 1 \right). \qquad (2.58)$$

The locations of stable and unstable circular orbits are identified by photon and antiphoton spheres, respectively. They satisfy the condition

$$\frac{C'}{C} - \frac{A'}{A} = 0. \qquad (2.59)$$

In a gravitational field, photons (light particles) are influenced by spacetime curvature, creating regions known as the photon and antiphoton spheres. These spheres represent specific distances from a massive object where light can orbit due to the gravitational potential.

- **Photon Sphere:** The photon sphere corresponds to the location where the effective potential reaches a maximum. Photons here experience a balance between gravitational pull and outward movement, allowing them to follow a (usually unstable) circular orbit. Mathematically, this is the radius r_{ph} where the second derivative of the effective potential, $\frac{d^2 V_{\text{eff}}}{dr^2}$, is positive, indicating a peak in the potential.

- **Antiphoton Sphere:** Conversely, the antiphoton sphere is region where the effective potential reaches a minimum, allowing for stable orbits. Here, $\frac{d^2 V_{\text{eff}}}{dr^2}$ is negative, showing a valley in the potential, which stabilizes the orbit.

The position of the photon sphere, denoted as r_{ph}, can be determined by solving a specific condition, as shown in (2.59). The photon and antiphoton spheres are essential for understanding gravitational lensing and light paths around dense objects like black holes.

Strong deflection due to photon Sphere

The bending angle will have the same expression as in (2.50) discussed in [50]. The expressions of $\bar{a}$ and $\bar{b}$ are same as described in (2.51). The subscript ph in the mentioned expression depicts the quantities at r_{ph} which is the radius of the photon sphere.

Strong deflection due to antiphoton Sphere

This behavior is observed in gravitational lensing caused by ultra-compact objects, where the effective potential for photons shows a distinct profile. As

photons approach the massive object, the effective potential first reaches a maximum at the photon sphere. Moving further, the potential decreases to a minimum at the antiphoton sphere, then increases below that radius.

When a photon has an impact parameter b less than the critical value b_{ph}, it crosses into the photon sphere. It continues and passes through the antiphoton sphere, where it turns within this region of minimum potential. Afterward, the photon exits the photon sphere and escapes, reaching a distant observer.

As the impact parameter b of a photon nears the critical value b_{ph}, the photon experiences significant gravitational deflection. To derive the strong deflection formula, we define a new variable z as follows:

$$z = 1 - \frac{r_{ph}}{r_t}. \tag{2.60}$$

Substituting the above value of z in $I(r_t)$, we obtain

$$I(r_t) = \int_z^1 f(z, r_t, r_{ph}) dz, \tag{2.61}$$

where

$$f(z, r_t, r_{ph}) = \frac{2r_{ph}}{\sqrt{X(z, r_t, r_{ph})}}, \qquad X(z, r_t, r_{ph}) = R\frac{C}{B}(1 - z^4). \tag{2.62}$$

By using (2.34), the expansion of $R(r)$ in the powers of z is as follows

$$R(r) = \left(\frac{A_t C_{ph}}{A_{ph} C_t} - 1\right) + \frac{r_{ph}^2}{2}\frac{A_t C_{ph}}{A_{ph} C_t}\left(\frac{C_{ph}''}{C_{ph}} - \frac{A_{ph}''}{A_{ph}}\right)z^2 + O(z^3). \tag{2.63}$$

Similar expansion will be done to obtain $X(z, r_t, r_{ph})$ in the powers of z as

$$X(z, r_t, r_{ph}) = \mathcal{A} + \mathcal{B}z + \mathcal{C}z^2 + O(z^3), \tag{2.64}$$

where

$$\mathcal{A} = \frac{C_{ph}}{B_{ph}}\left(\frac{A_t C_{ph}}{A_{ph} C_t} - 1\right), \tag{2.65}$$

$$\mathcal{B} = \frac{C_{ph}}{B_{ph}}\left(\frac{A_t C_{ph}}{A_{ph} C_t} - 1\right)\left[-4 + r_{ph}\left(\frac{C_{ph}'}{C_{ph}} - \frac{B_{ph}'}{B_{ph}}\right)\right], \tag{2.66}$$

and

$$\mathcal{C} = \frac{C_{ph}}{B_{ph}}\left(\frac{A_t C_{ph}}{C_t A_{ph}} - 1\right)\left[6 - r_{ph}\left(3 + \frac{B_{ph}' r_{ph}}{B_{ph}}\right)\left(\frac{C_{ph}'}{C_{ph}} - \frac{B_{ph}'}{B_{ph}}\right) + \frac{r_{ph}^2}{2}\left(\frac{C_{ph}''}{C_{ph}} - \frac{A_{ph}''}{A_{ph}}\right)\right]$$
$$+ \frac{r_{ph}^2}{2}\frac{C_{ph}}{B_{ph}}\frac{A_t C_{ph}}{A_{ph} C_t}\left(\frac{C_{ph}''}{C_{ph}} - \frac{A_{ph}''}{A_{ph}}\right). \tag{2.67}$$

When the critical impact parameter becomes close to the impact parameter from $b < b_{ph}$ side, a new radius r_c will be equal to the turning point r_t. Hence, in the limit $r_t \to r_c$, $\left(\frac{A_t C_{ph}}{A_{ph} C_t} - 1 \right) \to 0$. We obtain the following results by using the limit r_c

$$\mathcal{A}_{ph} = \mathcal{A}|_{r_t=r_c} = 0 = \mathcal{B}_{ph} = \mathcal{B}|_{r_t=r_c}, \qquad (2.68)$$

and

$$\mathcal{C}_{ph} = \mathcal{C}|_{r_t=r_c} = \frac{r_{ph}^2}{2} \frac{C_{ph}}{B_{ph}} \left(\frac{C_{ph}''}{C_{ph}} - \frac{A_{ph}''}{A_{ph}} \right). \qquad (2.69)$$

Finally, we obtain

$$X_{ph}(z) = \mathcal{C}_{ph} z^2 + O(z^3).$$

The nature of divergence is logarithmic in the strong deflection limit $r_t \to r_c$. To eliminate divergence, we will split the expression $I(r_t)$ to the divergent $I_D(r_t)$ and regular part $I_R(r_t)$. The divergent part is defined as

$$I_D(r_t) = \int_{1-\frac{r_{ph}}{r_t}}^{1} f_D(z, r_t, r_{ph}) dz, \quad f_D(z, r_t, r_{ph}) = \frac{2r_{ph}}{\sqrt{\mathcal{A} + \mathcal{B}z + \mathcal{C}z^2}}. \qquad (2.70)$$

$I_R(r_t)$ is defined as

$$I_R(r_t) \int_{1-\frac{r_{ph}}{r_t}}^{1} f_R(z, r_t, r_{ph}), \quad f_R(z, r_t, r_{ph}) = f(z, r_t, r_{ph}) - f_D(z, r_t, r_{ph}). \qquad (2.71)$$

The integration of $I_D(r_t)$ will give

$$I_D(r_t) = \frac{2r_{ph}}{\sqrt{\mathcal{B}_{ph}}} \log \frac{\mathcal{A} + 2\mathcal{B} + 2\sqrt{\mathcal{B}}\sqrt{\mathcal{A} + \mathcal{B} + \mathcal{C}}}{\mathcal{A} + 2\mathcal{B}\left(1 - \frac{r_{ph}}{r_t}\right) + 2\sqrt{\mathcal{B}}\sqrt{\mathcal{C} + \mathcal{A}\left(1 - \frac{r_{ph}}{r_t}\right) + \mathcal{B}(1 - \frac{r_{ph}}{r_t})^2}}. \qquad (2.72)$$

In the strong deflection limit $r_t \to r_c$ and taking $\mathcal{C}$ and $\mathcal{A}$ as small values,

the above expression reduces to

$$I_D(r_t) = \frac{2r_{ph}}{\sqrt{\mathcal{B}_{ph}}} \log \left[\frac{4\mathcal{B}_{ph}(\frac{r_{Ph}}{r_t} - 1)}{\frac{C_{ph}}{B_{ph}}\left(\frac{A_t C_{ph}}{C_t A_{ph}} - 1\right)} \right] + O\left[\left(\frac{A_t C_{ph}}{C_t A_{ph}} - 1 \right) \log \left(\frac{A_t C_{ph}}{C_t A_{ph}} - 1 \right) \right]. \qquad (2.73)$$

Using the expansion mentioned in (2.34)

$$A_t = A_c + A_c'(r_t - r_c) + O(r_t - r_c)^2,$$

32

and
$$C_t = C_c + C'_c(r_t - r_c) + O(r_t - r_c)^2,$$

we obtain
$$\frac{A_t C_{ph}}{C_t A_{ph}} = \frac{C_{ph}}{A_{ph}} \left[\frac{A_c + A'_c(r_t - r_c) + O(r_t - r_c)^2}{C_c + C'_c(r_t - r_c) + O(r_t - r_c)^2} \right],$$

where the subscript "c" represents quantities at $r = r_c$, and a condition $\frac{A_c C_{ph}}{A_{ph} C_c} = 1$ will be used in the expansion.

$$\frac{A_t C_{ph}}{C_t A_{ph}} = \frac{C_t}{A_t} \left[\frac{A_c}{C_c + C'_c(r_t - r_c)} + \frac{A'_c(r_t - r_c)}{C_c + C'_c(r_t - r_c)} + O(r_t - r_c)^2 \right],$$

$$= \frac{C_t A_c}{C_c A_t} \left[\frac{1}{1 + \frac{C'_c}{C_c}(r_t - r_c)} + \frac{A'_c/A_c(r_t - r_c)}{1 + \frac{C'_c}{C_c}(r_t - r_c)} \right] + O(r_t - r_c)^2.$$

Using the condition $\frac{A_c C_{ph}}{A_{ph} C_c} = 1$, we get

$$\frac{A_t C_{ph}}{C_t A_{ph}} = \left(1 + \frac{A'_c}{A_c}(r_t - r_c) \right) \left(1 + \frac{C'_c}{C_c}(r_t - r_c) \right)^{-1} + O(r_t - r_c)^2,$$

here, we use the binomial theorem and after a few simplifications

$$\frac{A_t C_{ph}}{C_t A_{ph}} = 1 + \left(\frac{A'_c}{A_c} - \frac{C'_c}{C_c} \right) (r_t - r_c) + O(r_t - r_c)^2. \qquad (2.74)$$

Using (2.73) and (2.74), we will get a new form of $I_D(r_t)$

$$I_D(r_t) = -\frac{2r_{ph}}{\sqrt{\mathcal{B}_{ph}}} \log(r_c - r_t) + \frac{2r_{ph}}{\sqrt{\mathcal{B}_{ph}}}$$

$$\log \left[4 \frac{B_{ph}}{C_{ph}} \left(\frac{r_{ph}}{r_c} - 1 \right) \mathcal{B}_{ph} \left(\frac{C'_c}{C_c} - \frac{A'_c}{A_c} \right)^{-1} \right] + O((r_t - r_c)\log(r_t - r_c)).$$

$$(2.75)$$

Writing I_D in terms of impact parameter b will be more convenient. First of all, we will consider some values related to the impact parameter $b(r_t) = \frac{C(r_t)}{A(r_t)}$ and $b(r_{ph}) = \frac{C_{ph}}{A_{ph}}$ and then from (2.74),

$$\frac{A_t C_{ph}}{C_t A_{ph}} - 1 = \left(\frac{A'_c}{A_c} - \frac{C'_c}{C_c} \right) (r_t - r_c),$$

$$(r_t - r_c) = \frac{-\frac{A_t C_{ph}}{C_t A_{ph}} + 1}{\left(\frac{A'_c}{A_c} - \frac{C'_c}{C_c} \right)}.$$

By using the above two expressions, we get

$$r_t = r_c - \left(\frac{C_c'}{C_c} - \frac{A_c'}{A_c} \right)^{-1} \left(\frac{b_{ph}^2}{b^2} - 1 \right). \tag{2.76}$$

Now, the value of I_D in strong field limits $b \to b_{ph}$ is calculated through (2.76)

$$I_D(b) = -\frac{2r_{ph}}{\sqrt{\mathcal{B}_{ph}}} \log \left(\frac{b_{ph}^2}{b^2} - 1 \right) + \frac{2r_{ph}}{\sqrt{\mathcal{B}_{ph}}} \log \left[4 \frac{B_{ph}}{C_{ph}} \left(\frac{r_{ph}}{r_c} - 1 \right) \mathcal{B}_{ph} \right]$$
$$+ O((b_{ph}^2 - b^2) \log(b_{ph}^2 - b^2)). \tag{2.77}$$

In the strong field limits, we will expand the regular part in the powers of $r_c - r_t$ and truncate the expression up to the leading order from which analytical and numerical values will be approximated. We find that

$$I_R(r_t) = \int_{1-\frac{r_{ph}}{r_c}}^{1} f_R(z, r_c, r_{ph}) dz + O((r_c - r_t) \log(r_t - r_c)). \tag{2.78}$$

It can be expressed in terms of impact parameter as

$$I_R(b) = \int_{1-\frac{r_{ph}}{r_c}}^{1} f_R(z, b_{ph}) dz + O((b_{ph}^2 - b^2) \log(b_{ph}^2 - b^2)). \tag{2.79}$$

Finally, the deflection angle is written as

$$\alpha(b) = -\bar{\tilde{a}} \log \left(\frac{b_{ph}^2}{b^2} - 1 \right) + \bar{\tilde{b}} + O((b_{ph}^2 - b^2) \log(b_{ph}^2 - b^2)), \tag{2.80}$$

where,

$$\bar{\tilde{a}} = 2 \sqrt{ \frac{2 B_{ph} A_{ph}}{C_{ph}'' A_{ph} - A_{ph}'' C_{ph}} }, \tag{2.81}$$

and

$$\bar{\tilde{b}} = \bar{a} \log \left[2 r_{ph}^2 \left(\frac{C_{ph}''}{C_{ph}} - \frac{A_{ph}''}{A_{ph}} \right) \right]. \tag{2.82}$$

The photon sphere formed by the equations above will be different from that formed in [50]. If we analyze both cases, the value of $\bar{a}$ is double in the case of the antiphoton sphere. The $\bar{b}$ also contain an extra term which is $\left(\frac{r_{ph}}{r_c} - 1 \right)$. Due to the presence of these terms, unlike the outer relativistic images, the bending angle for inner relativistic pictures begins to diverge before the critical impact parameter is attained. As a result, the angular distance between the inner images is significantly larger than the outside images.

2.4 Summary

This chapter explores the strong gravitational bending associated with a naked singularity, detailing its unique characteristics and behavior. The analysis extends to two other cases: one involving a spacetime that contains only a photon sphere, and another focusing on the gravitational lensing produced by ultracompact objects. We delve into the mechanisms of gravitational lensing and the resulting formation of relativistic images around these horizon-less ultracompact objects, drawing comparisons to similar phenomena around black holes.

For black holes, relativistic images form exclusively outside their photon spheres, but in contrast, horizon-less ultracompact objects have the potential to produce additional relativistic images within the radius of their photon spheres. This research introduces an analytical approach to understanding the pronounced gravitational lensing effects of ultracompact objects, presenting a novel perspective distinct from the methods typically applied to black holes, such as those in Bozza's work [53].

Chapter 3

Gravitational Lensing by a Dark Compact Object in Modified Gravity

Modified gravity theories emerged in the early twentieth century to address the limitations of Einstein's general theory of relativity (GR). While GR, introduced in 1915, effectively describes gravity as the curvature of spacetime induced by mass and energy, it struggles to account for significant astronomical phenomena, such as the rotation curves of galaxies, without invoking dark matter. Dark matter was proposed to explain the stable motion observed in galaxies and clusters of galaxies. However, GR cannot fully explain current astrophysical and cosmological observations without the inclusion of dark matter, which has yet to be detected in laboratory experiments [17].

Two alternative theories of gravity have been proposed to explain the rotational velocity curves of galaxies and clusters without resorting to dark matter: non-symmetric gravity theory (NGT) [17] and metric–skew–tensor gravity (MSTG) [18]. The final phase of a body's collapse can be attributed to an enhanced gravitational constant G and a gravitational repulsive force characterized by the charge $Q = \sqrt{\alpha} G_N M$, where α is a parameter defined as $G = G_N(1 + \alpha)$, G_N represents Newton's constant, and M is the total mass of the black hole [22]. Various solutions to Einstein's equations in modified gravity spacetimes are examined in [21–24]. A particular static, spherically symmetric solution in modified gravity, which features two event horizons, is discussed in [30]. In addition, the Kerr-MOG spacetime solution, which includes two event horizons and an ergosphere, is also explored. This solution is distinguished from the Schwarzschild solution by its line element, which incorporates a free parameter α.

3.1 Gravitational Lensing of Spacetime in Modified Gravity

3.1.1 Line Element of Spacetime in MOG

The line element of static, spherically symmetric spacetime in MOG is defined as [30]

$$ds^2 = f_s(r)dt^2 - \frac{1}{f_s(r)}dr^2 - r^2 d\Omega^2.$$

The line element describes the generally static, spherically symmetric, and asymptotically flat spacetime:

$$ds^2 = A(r)dt^2 - B(r)dr^2 - r^2 d\Omega^2.$$

Here,

$$A(r) = f_s(r), \qquad B(r) = \frac{1}{f_s(r)}, \qquad C(r) = r^2. \tag{3.1}$$

where $d\Omega^2 = d\theta^2 + \sin^2\theta\, d\phi^2$. The exact function $f_s(r)$ for the given spacetime in Modified Gravity (MOG) is [54]:

$$f_s(r) = 1 - \frac{2(1+\alpha)Mr^2}{(r^2 + \alpha(1+\alpha)M^2)^{\frac{3}{2}}} + \frac{\alpha(1+\alpha)M^2 r^2}{(r^2 + \alpha(1+\alpha)M^2)^2}.$$

A static, spherically symmetric solution in Modified Gravity (MOG) that remains regular at $r = 0$ is obtained. This solution features two horizons when $\alpha < \alpha_{\mathrm{crit}} = 0.673$. As r approaches 0, the metric effectively describes a De Sitter (or anti-De Sitter) spacetime. The asymptotic behavior of $f_s(r)$ for large r is:

$$f_s(r) = 1 - \frac{2(1+\alpha)M}{r} + \frac{\alpha(1+\alpha)M^2}{r^2} + O(M^3). \tag{3.2}$$

Here, α is a dimensionless parameter. Setting $\alpha = 0$ recovers the Schwarzschild coordinates from the given line element of a dark compact object in modified gravity. We will use $f_s(r)$, as defined in (3.2), throughout the process of finding the deflection angle.

3.1.2 Characteristics of Null Geodesics in Modified Gravity Spacetime

The properties of null geodesics in this spacetime will be investigated here. We can set $\theta = \pi/2$ without losing generality because it does not affect the spacetime symmetry due to the spherically symmetric property of spacetime. Furthermore, as a static, spherically symmetric spacetime, it admits two constants of motion: energy (E) and the z-component of angular momentum (ℓ). The geodesic equations for photon motion are as follows:

$$\dot{t} = \left(1 - \frac{2(1+\alpha)M}{r} + \frac{\alpha(1+\alpha)M^2}{r^2}\right)E, \quad \text{and} \quad \dot{\phi} = \frac{\ell}{r^2},$$

The overdot represents a derivative of the affine parameter along a null geodesic concerning the radial coordinate. The normalization criterion for photon four-velocity ($u^\mu u_\mu = 0$) yields:

$$\dot{r}^2 + \frac{\ell^2}{r^2}\left(1 - \frac{2(1+\alpha)M}{r} + \frac{\alpha(1+\alpha)M^2}{r^2}\right) = E^2,$$

or

$$\dot{r}^2 + V_{\text{eff}}(r) = E^2,$$

where

$$V_{\text{eff}}(r) = \frac{\ell^2}{r^2}\left(1 - \frac{2(1+\alpha)M}{r} + \frac{\alpha(1+\alpha)M^2}{r^2}\right),$$

is the effective potential for photon motion. At the turning point (r_t), we have $\dot{r} = 0$, which gives:

$$V_{\text{eff}}(r_t) = \frac{\ell^2}{r_t^2}\left(1 - \frac{2(1+\alpha)M}{r_t} + \frac{\alpha(1+\alpha)M^2}{r_t^2}\right) = E^2,$$

and

$$\frac{\ell}{E} = b(r_t) = \sqrt{(r_t + M)^2} = (r_t + M),$$

where $b = \ell/E$ represents the impact parameter of a light ray, which is a constant of motion for that ray. The effective potential is plotted against r in 3.1. the effective potential analysis reveals how varying the parameter α influences the existence and characteristics of photon spheres and affects gravitational lensing dynamics. This study is crucial for understanding the behavior of light around compact objects and provides insights into the gravitational influence of such celestial bodies.
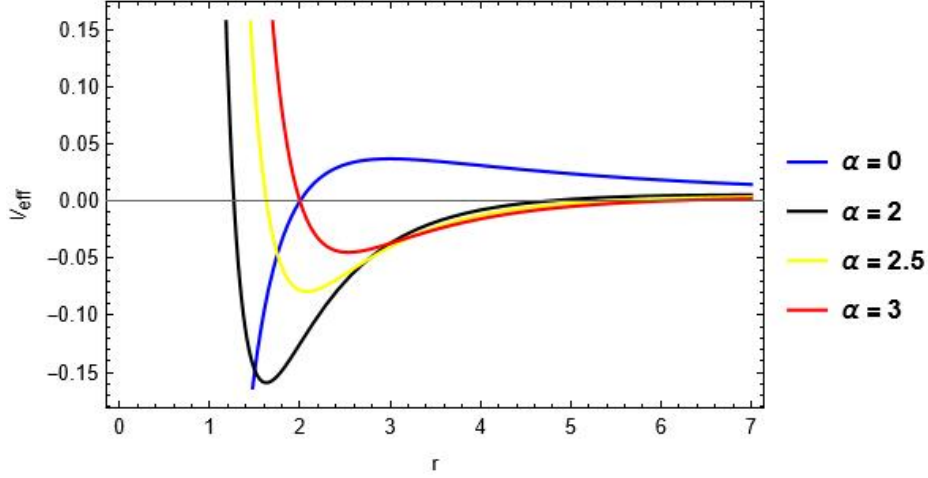
Figure 3.1: Effective potential is plotted against b for different values of α. The blue curve represents the Schwarzschild case when $\alpha = 0$. Other curves are drawn for mentioned values of α.

3.1.3 Weak Deflection Angle of Spacetime in MOG

To calculate the weak deflection angle of static spherically symmetric spacetime in MOG, the Gibbons and Werner method will be used [55]. According to their approach, for asymptotically flat spacetime, the following formula is applicable to find the weak deflection angle:

$$\alpha = - \int \int_{ph} K \, d\sigma. \tag{3.3}$$

Here, $d\sigma = \sqrt{\overline{g}_{rr}\,\overline{g}_{\phi\phi}}\, dr\, d\phi$ is an areal element and K is the Gaussian curvature of spacetime. The value of $\int k_g dl = 0$, because the spacetime is asymptotically flat. Hence, the geodesics curvature will be zero [56]. The optical metric for the given spacetime can be derived by considering the null geodesics condition, which is defined as $ds^2 = 0$:

$$f_s(r)\, dt^2 - \frac{1}{f_s(r)}\, dr^2 - r^2\, d\Omega^2 = 0.$$

Then, the optical metric has an expression:

$$dt^2 = \frac{1}{(f_s(r))^2}\, dr^2 + \frac{r^2}{f_s(r)}\, d\phi^2, \tag{3.4}$$

and

$$dt^2 = \overline{g}_{rr}\, dr^2 + \overline{g}_{\phi\phi}\, d\phi^2.$$

39

After finding the optical metric, one has to determine the Gaussian curvature K of the given spacetime. Gaussian Curvature tells us that the surface is curved. We will find the expression of Gaussian curvature using the optical metric $\overline{g}_{ij}$ instead of the given g_{ij}. By using the formula of Gaussian Curvature as described in [39], the value of K for the compact object in MOG is:

$$
\begin{aligned}
K &= -\frac{1}{\sqrt{\overline{g}_{rr}\,\overline{g}_{\phi\phi}}} \frac{\partial}{\partial r} \left(\frac{r^2 - 3Mr - 3Mr\alpha + 2M^2\alpha(1+\alpha)}{r^2 \sqrt{\frac{r^2 - 2Mr - 2Mr\alpha + M^2\alpha(1+\alpha)}{r^2}}} \right), \\
&= \frac{M(1+\alpha)\left(2r^3 + 6M^2 r\alpha(1+\alpha) - 2M^3\alpha^2(1+\alpha) - 3Mr^2(1+2\alpha)\right)}{r^5 \left(\frac{r^2 - 2Mr(1+\alpha) + M^2\alpha(1+\alpha)}{r^2} \right)^{3/2}}.
\end{aligned}
$$

Using the series expansion, we truncate it up to $O(M^3)$:

$$
K = -\frac{2M(1+\alpha)}{r^3} + \frac{3M^2(1+\alpha)(1+2\alpha)}{r^4} + O(M^3). \tag{3.5}
$$

The integration of Gaussian curvature over an infinite region will give the value of a weak deflection angle here. According to Gibbons and Werner's approach, the weak deflection angle of spacetime which is asymptotically flat can be calculated using the formula as in [55]:

$$
\alpha = -\int_0^\pi \int_{\frac{1}{r_\gamma}}^\infty K\,d\sigma. \tag{3.6}
$$

We want to find the expression of the bending angle up to the second order because higher order terms do not affect the overall weak deflection angle, we will find the expression of $\frac{1}{r_\gamma}$ accordingly. The light ray trajectory has an equation which is given up to $O(M^2)$, as seen in Equation (7) in [34]. The same approach will be used here. By considering the null geodesic condition $ds^2 = 0$ and using (2.54), we get

$$
\dot{r}^2 = E^2 - \frac{f_s(r)L^2}{r^2},
$$

and dividing it by $\dot{\phi}^2$ results in:

$$
\left(\frac{dr}{d\phi} \right)^2 = \frac{r^4}{b^2} - r^2 f_s(r).
$$

We will substitute $u = \frac{1}{r}$, and the above equation reduces to:

40

$$\left(\frac{du}{d\phi}\right)^2 = \frac{1}{b^2} - u^2 + 2(1+\alpha)Mu^3.$$

To obtain the trajectory of light up to $O(M^2)$, we will suppose a solution of the above equation as:

$$u = \frac{1}{b}(\sin\phi + u_1 M + u_2 M^2),$$

where u_1 and u_2 are corrections to the zeroth-order solution, representing the straight line $u_0 = \frac{1}{b}\sin\phi$. When we substitute the above expression into $\left(\frac{du}{d\phi}\right)^2$, two differential equations are obtained:

$$\frac{du_1}{d\phi} = -\frac{\sin\phi}{\cos\phi}u_1 + \frac{1}{2b}\frac{\sin^3\phi(1+\alpha)}{\cos\phi},$$

and

$$\frac{du_2}{d\phi} = -\frac{\sin\phi}{\cos\phi}u_2 - \frac{1}{2\cos\phi}\left[\left(\frac{du_1}{d\phi}\right)^2 - u_1^2 - \frac{3}{b}u_1\sin^2\phi(1+\alpha)\right].$$

The integration constants are chosen according to the condition about maximizing u for $\theta = \frac{\pi}{2}$. The final equation of trajectory up to the second order is:

$$\frac{1}{r_\gamma} = \frac{\sin\phi}{b} + \frac{M(1+\alpha)}{2b^2}(3 + \cos(2\phi))$$
$$+ M^2\left(\frac{3(5\pi - 2(5+11\alpha)\phi)\cos\phi + (17 + 39\alpha - (3+5\alpha)\cos(2\phi))\sin\phi}{8b^3}\right)$$
$$\tag{3.7}$$

Using (3.5) and (3.7) in (3.6), we obtain:

$$\hat{\alpha} = -\frac{M\left(5M\pi\alpha^2 + 768b^3(1+\alpha) + 144b^2 M\pi(1+\alpha)(5+4\alpha)\right)}{192b^4}.$$

The expansion of the above expression to the second order of alpha results in

$$\hat{\alpha} = \frac{4M}{b} + \frac{15\pi M^2}{4b^2} + \left(\frac{4M}{b} + \frac{27\pi M^2}{4b^2}\right)\alpha + \frac{3\pi M^2 \alpha^2}{b^2} + \cdots \tag{3.8}$$

When we substitute $\alpha = 0$ in (3.8), the weak deflection angle for the Schwarzschild black hole will be obtained.
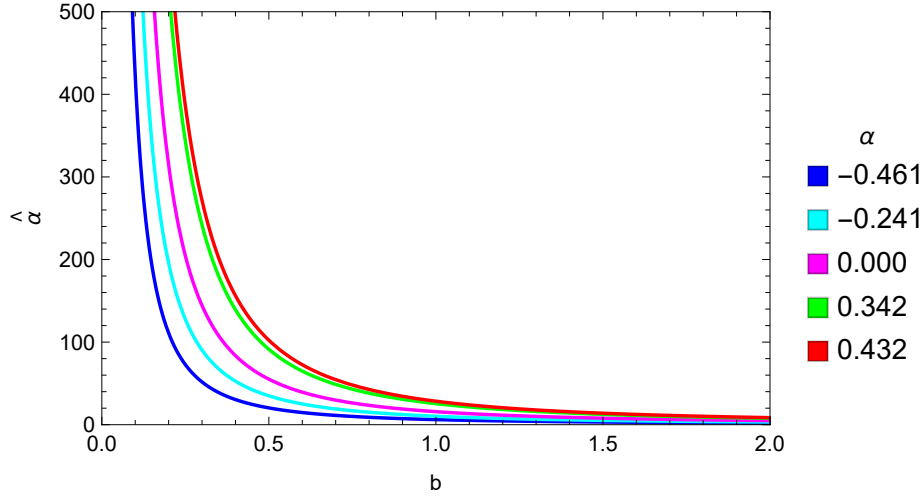
Figure 3.2: Weak deflection angle is plotted against different values of impact parameter b and α.

3.1.4 Strong Deflection Angle of Spacetime in MOG

The improved approach of Naoki Tsukamoto [50] will be used here to obtain the strong deflection angle of dark compact objects in MOG. The given spacetime has the following characteristics that are static, spherically symmetric, and asymptotically flat as it satisfies an asymptotic flatness. Using (3.1), we obtain

$$\lim_{r \to \infty} A(r) = 1, \tag{3.9}$$

$$\lim_{r \to \infty} B(r) = 1, \tag{3.10}$$

$$\lim_{r \to \infty} C(r) = r^2. \tag{3.11}$$

The radius of the photon sphere, impact parameter, and critical impact parameter are calculated by following the expressions given in the equations (2.8), (2.15), and (2.20) in [50], respectively. First of all, The radius of the photon sphere r_{ph} can be obtained by assuming that there exists at least one positive solution of $D(r) = 0$, where

$$D(r) = \frac{C'}{C} - \frac{A'}{A}. \tag{3.12}$$

By using the required values in (3.12)

$$\frac{2r}{r^2} - \frac{\frac{2M(1+\alpha)}{r^2} - \frac{2M^2\alpha(1+\alpha)}{r^3}}{1 - \frac{2(1+\alpha)M}{r} + \frac{\alpha(1+\alpha)M^2}{r^2}} = 0,$$

which yields

$$r_{ph} = \frac{1}{2}(3M + 3M\alpha + \sqrt{9M^2 + 10M^2\alpha + M^2\alpha^2}). \qquad (3.13)$$

(3.13) shows the radius of the photon sphere. Secondly, the impact parameter is defined as

$$b = \sqrt{\frac{C_t}{A_t}}.$$

The subscript t denotes the quantities at $r = r_t$ throughout the dissertation which is the closest approached distance of the light ray near the lens. Critical impact parameter has the following mathematical form

$$b_c = \lim_{r_t \to r_{ph}} \sqrt{\frac{C_t}{A_t}},$$

$$= \lim_{r_t \to r_{ph}} \sqrt{\frac{r_t^2}{1 - \frac{2M(1+\alpha)}{r_t} + \frac{\alpha(1+\alpha)}{r_t^2}}},$$

$$b_c = \frac{\sqrt{2}(3M + 3M\alpha + M^2(9 + 10\alpha + \alpha^2))^2}{4((1+\alpha)M(3M + M\alpha + \sqrt{M^2(9 + 10\alpha + \alpha^2)}))}.$$

After a few simplifications, we obtain

$$b_c = 3\sqrt{3}M + \frac{5}{2}\sqrt{3}M\alpha - \frac{7}{24\sqrt{3}}M\alpha^2 + O(M^3). \qquad (3.14)$$

Deflection angle in [50] is given by the expression

$$\hat{\alpha} = \bar{a}\log\left(\frac{b}{b_c} - 1\right) + \bar{b} + O((b - b_c)\log(b - b_c)), \qquad (3.15)$$

where $\bar{a}$ and $\bar{b}$ are defined as

$$\bar{a} = \sqrt{\frac{2B_{ph}A_{ph}}{C''_{ph}A_{ph} - A''_{ph}C_{ph}}}, \qquad (3.16)$$

and

$$\bar{b} = \bar{a}\log\left[r_{ph}^2\left(\frac{C''_{ph}}{C_{ph}}\frac{A''_{ph}}{A_{ph}}\right)\right] + I_R(r_{ph}) - \pi. \qquad (3.17)$$

Substituting the values of $A(r)$, $B(r)$, and $C(r)$ from (3.1) into (3.16), we get
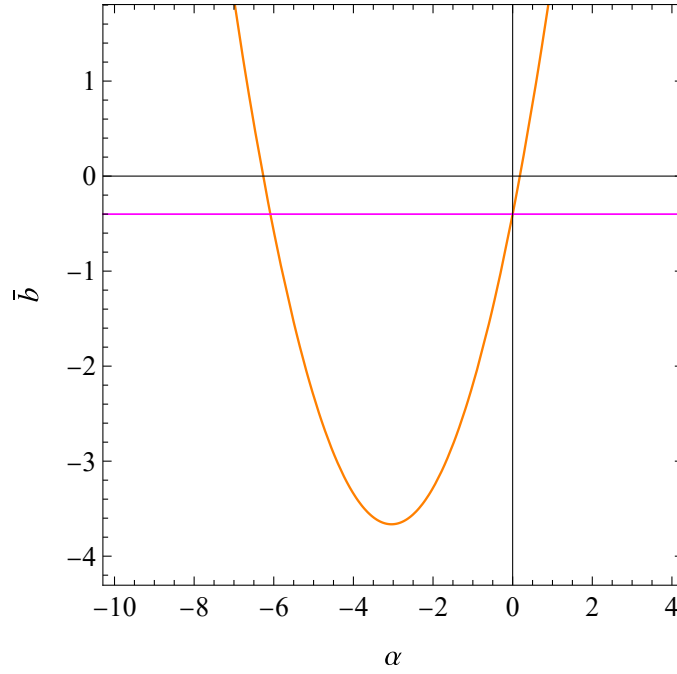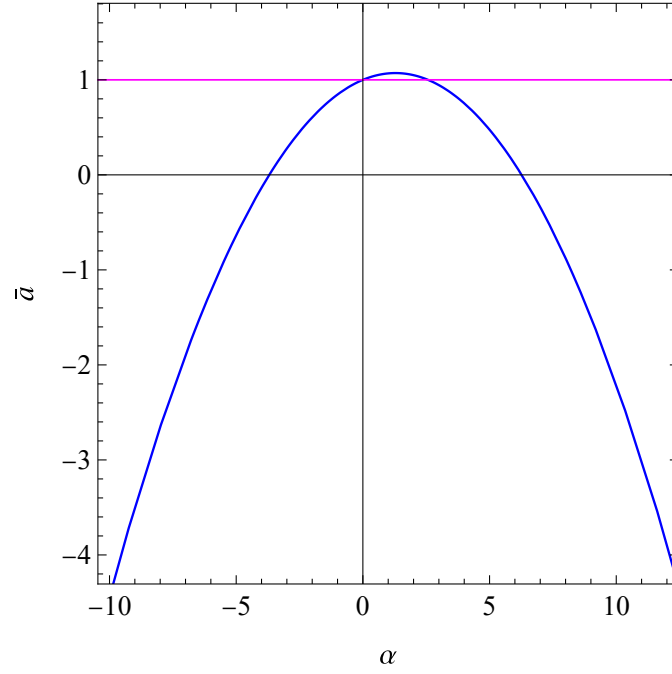
Figure 3.3: The lensing coefficients $\overline{a}$ and $\overline{b}$ are plotted against the impact parameter b. The magenta line represents the Schwarzschild case in both plots.

$$\bar{a} = \frac{\sqrt{M}(9 + 5\alpha + 3\sqrt{9 + 10\alpha + \alpha^2})}{\sqrt{2}\sqrt{M(81 + 72\alpha + 7\alpha^2 + 9(3 + \alpha)\sqrt{9 + 10\alpha + \alpha^2})}}.$$

After applying the series expansion on the above expression, a more simplified version is

$$\bar{a} = 1 + \frac{\alpha}{9} - \frac{7\alpha^2}{162} + O(\alpha^3). \tag{3.18}$$

Using equation (3.17), the value of $\bar{b}$ is as follows

$$\bar{b} = \frac{1}{9}\alpha(-1 + \log[6]) + \log[6] - \frac{1}{162}\alpha^2(-5 + \log[279936]) + I_R(r_{ph}) - \pi. \tag{3.19}$$

$I_R(r_{ph})$ is obtained by using (2.48) in [50]. It has the following value

$$\begin{aligned}
I_R(r_{ph}) = &\frac{2}{9}\alpha(-6 + 6\sqrt{3} + \log(3 - \sqrt{3})) + 2\log[6(-\sqrt{3} + 2)] \\
&- \frac{\alpha^2}{81}(-146 + 74\sqrt{3} + \log[279936] - 7\log(3 + \sqrt{3})).
\end{aligned} \tag{3.20}$$

Using (3.16), (3.17), and (3.20) in (3.15), we can obtain the strong deflection angle of light rays of dark compact objects in modified gravity as

$$\begin{aligned}
\hat{\alpha} = &\log(6) - \pi - \left(1 - \frac{b}{b_c}\right) + 2\log[-6(-2 + \sqrt{3})] \\
&+ \alpha\left[-\frac{1}{9}\left(\frac{b}{b_c} - 1\right) + \frac{1}{9}(-1 + \log[6])\right. \\
&\left. + \frac{2}{9}\left(-6 + 6\sqrt{3} + \log[3 - \sqrt{3}]\right)\right] \\
&+ \alpha^2\left[\frac{7}{162}\left(\frac{b}{b_c} - 1\right) - \frac{1}{162}(-5 + \log[279936])\right. \\
&\left. - \frac{1}{81}\left(-146 + 74\sqrt{3} + \log[279936] - 7\log[3 + \sqrt{3}]\right)\right].
\end{aligned} \tag{3.21}$$

When we substitute $\alpha = 0$ in (3.21), the strong deflection angle of Schwarzschild spacetime will be obtained [57]. The graph of lensing coefficients $\bar{a}$ and $\bar{b}$ are plotted against different values of impact parameter b shown in figure 3.3.

The purple line in the above graph represents the Schwarzschild case for the lensing coefficient $\bar{a}$. But in MOG, the linear term in $\bar{a}$ (3.18) dominates for small values of α, and the function will initially increase as α increases.
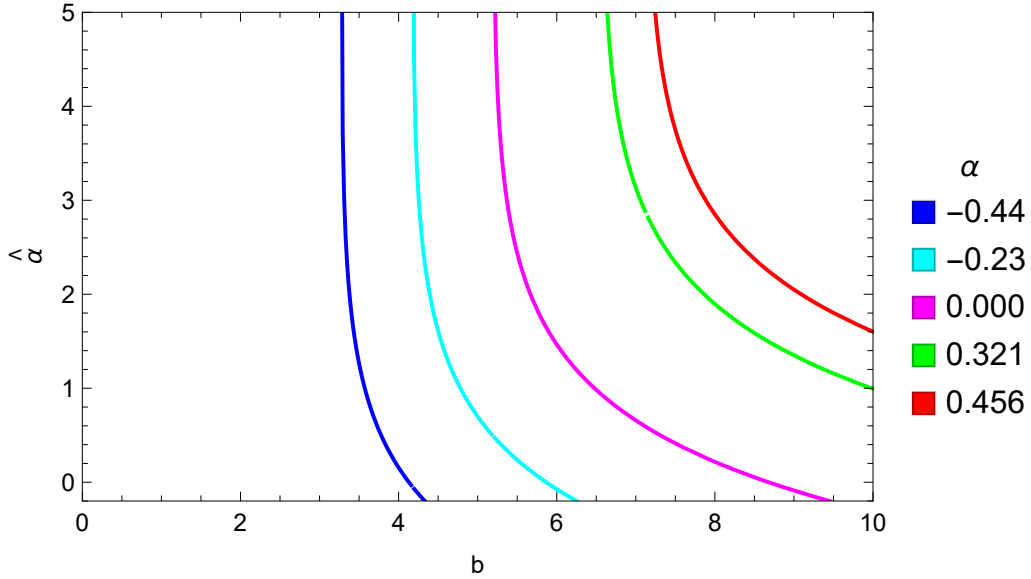
Figure 3.4: The strong deflection angle is plotted against different values of b.

For larger values of α, the quadratic term becomes more dominant, causing the function to bend downwards due to the negative coefficient of α^2.

The blue line in the graph below in figure 3.3 represents the lensing coefficient $\bar{b}$ in Schwarzschild spacetime. For small values of α, the linear term $\frac{1}{9}\alpha\left(-1 + \log[6]\right)$ dominates, causing the function $\bar{b}$ to increase approximately linearly with α. For larger values of α, the quadratic term becomes more significant and begins to overpower the linear term. Because this term is negative, it will cause the graph to bend downwards after a certain value of α, resulting in a concave down curve. The graph of strong deflection angle against different values of b is plotted in Figure 3.4. As α increases, the strong deflection angle also increases.

3.2   Observable in Strong Gravity

The strong field limit approximation can be used to calculate the deflection angle of light which involves logarithmic and constant terms. The main observable in the strong field limit is obtained just by substituting the specific values of given spacetime in the equation as described in [49]:

$$\hat{\alpha} = -\overline{\alpha} \log\left(1 - \frac{\vartheta D_{ol}}{u_{ph}}\right) + \overline{b}. \tag{3.22}$$

The lens equation defined in [53] is:

$$\beta = \vartheta - \frac{D_{ls}}{D_{os}}\Delta\alpha, \tag{3.23}$$

where D_{ls} denotes the distance between the lens and the source, β and ϑ represent the angular distances from the optical axis to the source and image, respectively, and $\Delta\hat{\alpha}_n = \hat{\alpha} - 2n\pi$ signifies the adjustment of the deflection angle after accounting for n loops of photons around the lens.

To transition from the deflection angle $\hat{\alpha}$ to the offset $\Delta\hat{\alpha}$, it is necessary to determine the value of ϑ_n^0 that satisfies the equation $\hat{\alpha}(\vartheta_n^0) = 2n\pi$. This condition implies that the deflection angle at ϑ_n^0 corresponds to an integral multiple of 2π, accounting for the number of loops n that photons make around the lens. By solving the equation $\hat{\alpha}(\vartheta_n^0) = 2n\pi$ (which refers to a previously defined equation, labeled as (3.22)), we can derive the corresponding offset $\Delta\hat{\alpha}$.

$$\vartheta_0^n = \frac{u_{ph}}{D_{ol}}\left(1 + e_n\right), \tag{3.24}$$

where

$$e_n = e^{\frac{\overline{b}-2n\pi}{\overline{a}}}.$$

$\Delta\hat{\alpha}_n$ can be determined by expanding $\alpha(\vartheta)$ in power of ϑ_n^0. By putting $\vartheta - \vartheta_n^0 = \Delta\vartheta_n$, the following expression obtained in [49]:

$$\Delta\alpha_n = -\frac{\overline{a}D_{ol}}{u_{ph}e_n}\Delta\vartheta_n. \tag{3.25}$$

Using (3.24) and (3.25) in (3.22) yields:

$$\beta = (\vartheta_n^0 + \Delta\vartheta_n) + \left(-\frac{\overline{a}D_{ol}}{u_{ph}e_n}\frac{D_{ls}}{D_{os}}\right)\Delta\vartheta_n. \tag{3.26}$$

Further, the approximation $u_{ph} = \tan\vartheta D_{ol} \approx \vartheta D_{ol}$ will be used along with (3.25) to obtain the nth position of relativistic images as:

$$\vartheta_n = \vartheta_n^0 + \frac{u_{ph}e_n(\beta - \vartheta_n^0)D_{os}}{\overline{a}D_{ls}D_{os}}. \tag{3.27}$$

When $n \to \infty$ in (3.27), $e_n \to 0$ such that $u_{ph} = \vartheta_\infty D_{ol}$. When $\beta = 0$, that is the lens, source, and object are perfectly aligned, we obtain the position

of n relativistic Einstein rings as:

$$\vartheta_n^E = \frac{u_{ph}}{\mathrm{D}_{ol}}\left(1 + e_n\right),$$

$$\vartheta_n^E = \frac{\frac{3\sqrt{3}}{2} + \frac{5\sqrt{3}\alpha}{4} - \frac{7\alpha^2}{48\sqrt{3}}}{\mathrm{D}_{ol}}\left(1 + e^{\frac{\bar{b}-\pi}{\bar{a}}}\right).$$

$$(3.28)$$

Note that $n = 1$ corresponds to the outermost relativistic ring. The Einstein rings for the two black holes are plotted against different values of α shown in figures 3.7 and 3.5. We plotted four Einstein rings for M87* black hole acting as a lens in modified gravity.

The magnification of the images can be calculated as in [49]:

$$\mu_n = \frac{1}{\beta}\left[\frac{u_{ph}}{\mathrm{D}_{ol}}\left(1 + e_n\right)\left(\frac{\mathrm{D}_{os}}{\mathrm{D}_{ls}}\frac{u_{ph}e_n}{\bar{a}\mathrm{D}_{ol}}\right)\right]. \qquad (3.29)$$

It is clear from (3.29) that if $\beta \to 0$, then the magnification $\mu_n \to \infty$, which shows that magnification is maximum in the case of perfect alignment of lens, source, and object. (3.29) relates the magnification with the image and source positions. The magnification of Einstein rings is plotted on figures 3.6 and 3.8.

In our analysis, we designate ϑ_1 as the angle corresponding to the outermost image produced by gravitational lensing. The remaining observed images are collectively represented by the angle ϑ_∞, which typically corresponds to the limiting case where the images converge. To characterize the lensing effect quantitatively, we will define three lensing coefficients based on the framework established in the work by Bozza [49]. These coefficients provide insight into the nature and strength of the lensing phenomenon.

$$u_{ph} = \frac{\vartheta_\infty}{\mathrm{D}_{ol}}, \qquad (3.30)$$

$$s = \vartheta_1 - \vartheta_\infty \approx \vartheta_\infty(e_n), \qquad (3.31)$$

$$r_{mg} = \exp\left(\frac{2\pi}{\bar{a}}\right). \qquad (3.32)$$

In this context, s represents the separation between the outermost and innermost images, marking the boundary of the shadow region, while r_{mg} denotes the ratio of the magnification of the first image compared to the higher-order images.

3.2.1 Analysis of Einstein Ring Radius for M87* in Modified Gravity

The Einstein ring radius represents the apparent size of the ring-like image formed by light bending around the supermassive black hole M87* in gravitational lensing. In the context of modified gravity, the relationship between the Einstein ring radius and the parameter α (which reflects deviations from general relativity) offers important insights into how gravity behaves in extreme environments.

Figure 3.5: The Einstein ring is plotted for the different values of α. The blue circle represents Einstein's ring in the Schwarzschild case. For this ring, we substitute $\alpha = 0$ in the expression of ϑ_E in modified gravity.

As the value of α increases from zero, which implies standard general relativity, the Einstein ring radius grows, showing that modified gravity enhances the bending of light. The following values are observed:

- When $\alpha = 0$, the Einstein ring radius is 19.8411.

- When $\alpha = 0.1$, the Einstein ring radius increases to 21.497.

- When $\alpha = 0.673$, the Einstein ring radius jumps to 30.8878.

- When $\alpha = 0.9$, the Einstein ring radius reaches 34.6736.
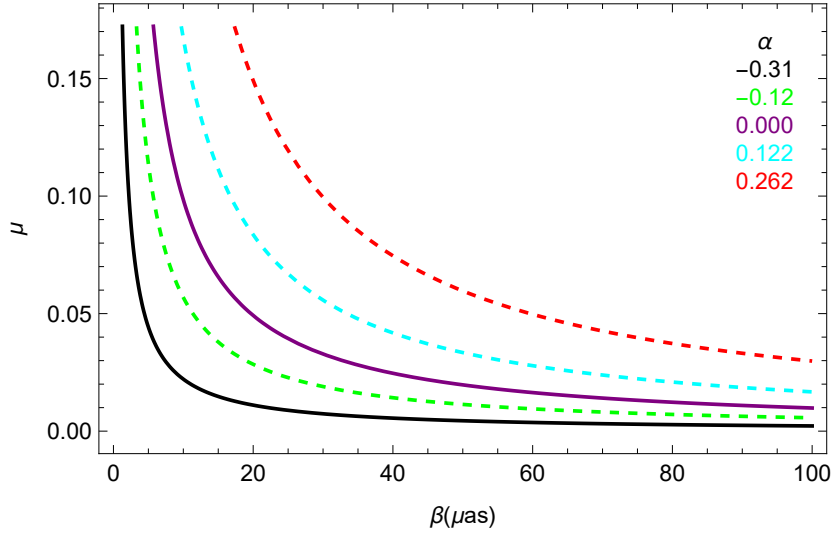
Figure 3.6: The magnification of the Einstein ring is plotted against different values of β. Here, the graph is drawn for the case when M87* acts as a lens in the modified gravity.

This trend demonstrates that even small changes in α lead to significant increases in the Einstein ring radius, indicating a stronger lensing effect in the presence of modified gravity. For instance, the radius grows from 19.8411 at $\alpha = 0$ (consistent with general relativity) to 34.6736 at $\alpha = 0.9$.

The graph of this relationship reveals a non-linear increase in the Einstein ring radius as α increases, showing how modifications to gravity can dramatically influence the curvature of spacetime around black holes like M87*. This suggests that further exploration of modified gravity models could provide new insights into the behavior of black holes and the nature of gravitational interactions in extreme conditions.

The lensing coefficients given in (3.30) and (3.31), are calculated along with other parameters in Table 3.1. The table highlights key changes in gravitational lensing and strong field properties of the black hole M87* under modified gravity compared to a Schwarzschild black hole. As the parameter representing modifications to gravity increases, the size of the Einstein ring and the separation between light rays grow, indicating stronger lensing effects. The photon sphere also expands, reflecting a larger region where light cannot escape the black hole's gravity. Additionally, the coefficients that describe how light is bent show a gradual shift, depicting how modified gravity alters the behavior of light around M87*, diverging from general relativity predictions.

	Schwarzschild BH	M87* in Modified Gravity			
α	0	0.2	0.4	0.6	0.8
$\vartheta_\infty(\mu\text{as})$	19.82	23.09	26.32	29.49	32.62
$s(\mu\text{as})$	0.0248	0.0510	0.1013	0.1961	0.3742
$\frac{u_{ph}}{r_s}$	2.6	2.81	3.45	3.68	4.28
$\bar{a}$	1	1.01	1.02	1.03	1.037
$\bar{b}$	-0.4002	-0.18	0.04	0.28	0.514

Table 3.1: This table estimates the primary observable and the strong field limit coefficients for the black hole M87* in the galaxy's center, considering various values of α for spacetime in modified gravity. $M = 6.5 \times 10^9$ and $D_{ol} = 16.8$ Mpc are used here. The terms ϑ_∞ and s are defined in the text. The value r_{ph} is represented as r in the magnitude form. $\bar{a}$ and $\bar{b}$ are the strong field limit coefficients and r_s is the Schwarzschild radius.

3.2.2 Analysis of Einstein Ring Radius for Sgr A* in Modified Gravity

The Einstein ring radius is a key feature in gravitational lensing, depicting the apparent size of the light ring formed around a massive object like the black hole Sgr A*. When considering modified gravity, the behavior of the Einstein ring radius changes as a function of the parameter α, which indicates deviations from general relativity.

For Sgr A*, as α increases from zero, the Einstein ring radius also grows, reflecting enhanced light bending in the modified gravity framework. The observed values are as follows:

- When $\alpha = 0$, the Einstein ring radius is 25.6406.

- When $\alpha = 0.1$, the radius increases to 27.7805.

- When $\alpha = 0.673$, the radius rises significantly to 39.9161.

- When $\alpha = 0.9$, the radius reaches 44.8086.

This progression highlights that even slight increases in α lead to a noticeable enlargement of the Einstein ring radius. For example, when $\alpha = 0$, consistent with general relativity, the radius is 25.6406. However, at $\alpha = 0.9$, the radius grows to 44.8086, showing a significant difference due to modified gravity effects.
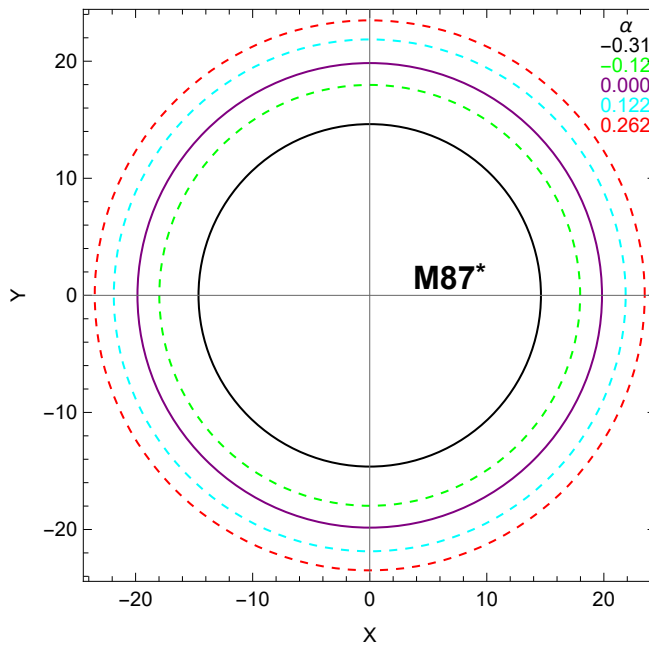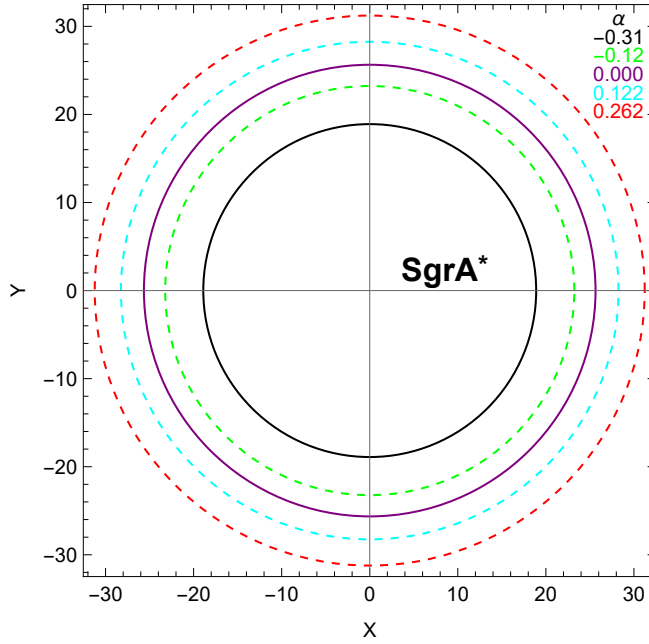
Figure 3.7: The Einstein ring is plotted for the different values of α. The blue circle represents Einstein's ring in the Schwarzschild case. For this ring, we substitute $\alpha = 0$ in the expression of ϑ_E in modified gravity.

The graph reveals that the radius of Einstein rings increases rapidly, especially as α approaches higher values, showing that deviations from general relativity affect the curvature of space around Sgr A^*. This provides important clues about how gravity might behave in extreme environments like the vicinity of black holes. Investigating such modifications to gravity could offer new insights into the nature of spacetime around Sgr A^* and other massive objects.

The table 3.2 compares the gravitational lensing properties of the black hole Sgr A^* in modified gravity with a Schwarzschild black hole. As the parameter for modified gravity increases, the size of the Einstein ring around Sgr A^* becomes larger, indicating stronger light bending. The separation between light rays also grows, suggesting more dominant lensing effects. The coefficients that describe how light bends change gradually, showing that the behavior of light around Sgr A^* differs significantly from predictions based on general relativity, as the modifications to gravity become more prominent.

	Schwarzschild BH	Sgr A* in Modified Gravity			
α	0	0.2	0.4	0.6	0.8
$\theta_\infty(\mu\mathrm{as})$	25.61	29.84	34.01	38.11	42.15
$s(\mu\mathrm{as})$	0.0248	0.0510	0.1013	0.1961	0.3742
$\frac{u_{ph}}{r_s}$	2.6	2.81	3.45	3.68	4.28
$\bar{a}$	1	1.01	1.02	1.03	1.037
$\bar{b}$	-0.4002	-0.18	0.04	0.28	0.514

Table 3.2: $M = 4 \times 10^6$ and $\mathrm{D}_{ol} = 0.008\mathrm{Mpc}$ is used here. $\bar{a}$ and $\bar{b}$ are the strong field limit coefficients and r_s is the Schwarzschild radius.
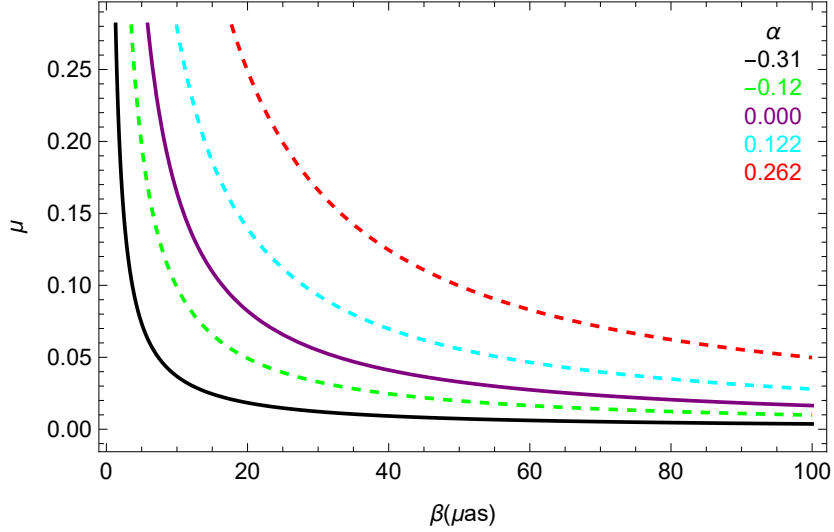
Figure 3.8: The magnification of the Einstein ring is plotted against the different values of β. Here, the graph is drawn for the case when Sgr A* acts as a lens in the modified gravity.

3.3 Lens Equation, Magnification and Distortion Parameter for Spacetime in Modified Gravity

To explore the phenomenon of gravitational lensing in both weak and strong gravitational fields, a lens equation was proposed in [42] as

$$\tan\beta = \tan\vartheta - \alpha, \tag{3.33}$$

where

$$\alpha = \frac{\mathrm{D}_{LS}}{\mathrm{D}_{OS}} \tan(\hat{\alpha} - \vartheta).$$

The angular position of the image and the angular position of the source are denoted by symbols ϑ and β respectively. D_{OS} is the observer-source distance and D_{LS} is the distance between the lensing object and the source. $\hat{\alpha}$ is the Einstein bending angle of the light ray. The angular position of the Einstein ring can be calculated by taking $\beta = 0$ in Equation (3.33). The impact parameter can be written in the form of ϑ as

$$b = \mathrm{D}_{ol} \sin\vartheta. \tag{3.34}$$

D_{ol} is the observer-lens distance. The radial magnification μ_r, the tangential magnification μ_t, and total magnification μ of the image can be expressed as

$$\mu_r = \left(\frac{d\beta}{d\vartheta}\right)^{-1}, \qquad \mu_t = \left(\frac{\sin\beta}{\sin\vartheta}\right)^{-1}, \qquad \mu = \mu_t\mu_r. \tag{3.35}$$

The Distortion Parameter is defined in [31] as

$$\Delta = \frac{\mu_t}{\mu_r}. \tag{3.36}$$

Also, a logarithmic distortion parameter of the image is defined in [31] as

$$\delta = \log_{10}\left|\frac{\mu_t}{\mu_r}\right|. \tag{3.37}$$

We will consider the simplest gravitational lensing i.e., the weak field lensing in modified gravity. (3.33) reduces to the well-known form [8]

$$\beta = \vartheta - \hat{\alpha}D, \tag{3.38}$$

where the bending angle is $\hat{\alpha} = \frac{4M}{b} + \frac{4M}{b}\alpha$. Solving equation (3.35) gives us the angular position of primary and secondary images as

$$
\begin{aligned}
\vartheta_p &= \frac{1}{2}(\beta + \sqrt{\beta^2 + 4\vartheta_E^2}), \\
\vartheta_s &= \frac{1}{2}(\beta - \sqrt{\beta^2 + 4\vartheta_E^2}),
\end{aligned}
\tag{3.39}
$$

where the angular radius of Einstein ring $\vartheta_E = \sqrt{\frac{4DM}{\mathrm{D}_{ol}}(1+\alpha)}$. Using (3.34) and (3.33) in (3.35), the distortion of the primary and secondary images will be obtained

$$
\Delta_p = -\Delta_s = \frac{\sqrt{\beta^2 + 16D\frac{M}{D}}}{\beta}.
\tag{3.40}
$$

The subscripts p and s are used for the primary and secondary relativistic images, respectively. The primary image ϑ_p is typically the first and brightest image formed by the lensing effect, on the other hand, the secondary image ϑ_s appears at a different angular position and is often fainter due to gravitational time delays, and the lensing geometry. These images arise from the bending of light around massive objects and are crucial for understanding the lensing properties and mass distribution of the lensing body.

3.4 Observable in the Weak Field Limit

To better understand the shapes of images in spacetime in modified gravity, we examine the variations in tangential and radial magnifications, as well as the total magnifications of the primary, secondary, and first- and second-order relativistic images (on both sides of the optic axis) against β, D, and $\frac{M}{\mathrm{D}_{ol}}$. While these investigations are now purely theoretical, they may someday yield useful insights into the properties of both the lenses and the sources [31].

We begin by modeling $M87^*$ (mass $M = 6.5 \times 10^9 M_\odot$ and distance $\mathrm{D}_{ol} = 16.8\mathrm{Mpc}$) as a Schwarzschild lens to examine lens-source gravitational lensing. A small value of $D = 0.005$ is utilized for our computations on relativistic images. For the $M87^*$ lens under modified gravity with $D = 0.005$, M/D_{ol} is around 3.68052×10^{-9}. The lens equation is valid because we are studying the weak field.

The graphs of tangential magnification for primary and secondary images are drawn in Figures 3.9-3.14. The tangential magnification for the primary

image (μ_{pt}) and secondary image (μ_{st}) is plotted against D, which represents the ratio of observer-lens distance to lens-source distance. In the context of modified gravity spacetime, α is a free parameter with various assigned values. When $\alpha = 0$, the scenario corresponds to the Schwarzschild case. As the value of α increases, both μ_{pt} and μ_{st} increase. Similarly, when plotted against β, representing the angular separation of the source, both μ_{pt} and μ_{st} also increase with increasing α.

Furthermore, plotting μ_{pt} and μ_{st} against M/D_{ol}, representing the ratio of the massive body to observer-lens distance, shows that both μ_{pt} and μ_{st} increase as M/D_{ol} increases. The radial magnification of the primary (μ_{pr}) and secondary (μ_{sr}) images is plotted against D, β, and M/D_{ol}. In all cases, the value of μ_{pr} decreases with an increase in the respective parameters and α, while μ_{sr} also decreases under the same conditions. Finally, the total magnification of the primary and secondary images is plotted against D. This total magnification increases as D and α increase, a trend that is consistent across different plotting variables, including β and M/D_{ol}.

3.5 Time Delay in SDL

Time delay in gravitational physics describes the phenomenon in which light or other signals take more time to traverse curved spacetime near a massive object than they would in flat spacetime. This effect is especially relevant in the framework of general relativity, where the presence of mass and energy alters the curvature of spacetime.

Using the approach outlined by [58], the time delay between the relativistic images is calculated. This delay occurs because photons follow distinct winding paths around the black hole, leading to a time difference between images formed on opposite sides of the lens. Given that the images are highly de-magnified and separated by only a few microarcseconds (μas), it is crucial to distinguish the outermost image from the others. For spherically symmetric black holes, when both images are on the same side of the source, the time delay between the first and second relativistic images is given by [58] as:

$$\Delta T_{2,1}^s = 2\pi b_c = 2\pi D_{OL}\theta_\infty. \tag{3.41}$$

The time delay for twenty-one different galaxies is calculated in Table 3.3. For M87*, the time delay will reach $\sim$9.804 min and $\sim$11.587 min for $\alpha = -0.1$ and $\alpha = 0.1$ in modified gravity, respectively. It can be observed that the positive values of α cause photons to experience greater gravitational

56

Galaxy	$M(M_\odot)$	D_{OL} (Mpc)	$\alpha = -0.1$	$\alpha = 0$	$\alpha = 0.1$
Milky Way	4.0×10^6	0.008	9.804	10.699	11.587
M87	6.5×10^9	16.8	15931.23	17385.67	18828.84
NGC 4472	2.54×10^9	16.72	6225.34	6793.78	7357.73
NGC 1332	1.47×10^9	22.66	3602.908	3931.84	4258.11
NGC 4374	9.25×10^8	18.51	2267.14	2474.11	2679.49
NGC 1399	8.81×10^8	20.85	2159.294	2356.43	2552.03
NGC 3379	4.16×10^8	10.70	1019.60	1112.68	1205.04
NGC 4486B	6×10^8	16.26	1470.58	1604.83	1738.05
NGC 1374	5.90×10^8	19.57	1446.07	1709.08	1578.08
NGC 4649	4.72×10^9	16.46	11568.52	12624.671	13672.64
NGC 3608	4.65×10^8	22.75	1139.70	1243.74	1346.99
NGC 3377	1.78×10^8	10.99	436.27	476.099	515.62
NGC 4697	2.02×10^8	12.54	495.09	540.29	585.14
NGC 5128	5.69×10^7	3.62	139.46	152.19	168.82
NGC 1316	1.69×10^8	20.95	414.21	452.03	489.55
NGC 3607	1.37×10^8	22.65	335.78	366.44	396.85
NGC 4473	0.90×10^8	15.25	220.59	240.72	260.71
NGC 4459	6.96×10^7	16.01	170.59	186.16	201.61
M32	2.45×10^6	0.8057	6.01	6.55	7.10
NGC 4486A	1.44×10^7	18.36	35.29	38.52	41.70
NGC 4382	1.30×10^7	17.88	31.86	34.77	37.66

Table 3.3: Estimation of time delay between the first and second relativistic image for supermassive black holes at the center of nearby galaxies. Mass (M) and distance (D_{OL}) are given in units of solar mass and Mpc, respectively [1]. Time delays are measured in minutes.

influence, thereby increasing the delay between different relativistic images in MOG while the reverse for negative values of α. Time delay for Sgr A* is not greater in MOG but for other galaxies, it is significant and can studied easily.

3.6 Summary

In this chapter, we explore several critical aspects of spacetime within the framework of Modified Gravity (MOG). We begin with the line element of spacetime in MOG, which provides the foundation for understanding how spacetime is structured under this theory. Following this, we delve into the weak deflection angle of spacetime in MOG, analyzing how light bends in the

presence of weak gravitational fields. This leads us to the study of the strong deflection angle, where we consider the behavior of light in strong gravitational fields, a crucial aspect for understanding phenomena near massive objects like black holes.

We then examine observable in strong gravity, identifying measurable quantities that can provide insights into the nature of gravity under strong field conditions. We also discuss the magnification and distortion parameters for spacetime in modified gravity, which are essential for understanding how images of distant objects are altered due to gravitational lensing. The chapter concludes with an analysis of observable in the weak field limit, detailing how gravitational effects can be measured and observed when the gravitational fields are relatively weak.
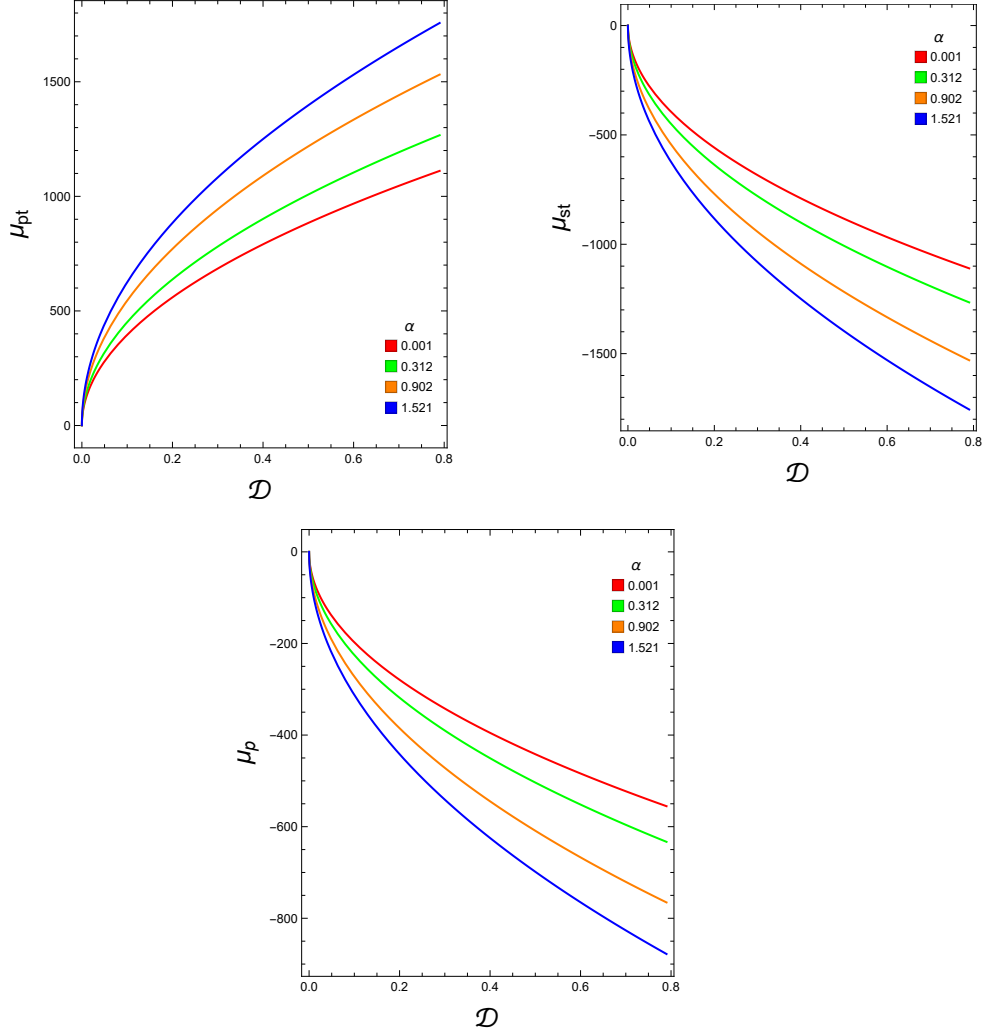
Figure 3.9: The tangential magnification variations for the distinct values of α and $\mathcal{D}$ are plotted here. 1st Row: The tangential magnification for the primary image (μ_{pt}) is plotted against $\mathcal{D}$ which represents the ratio of observer-lens distance to lens-source distance. In the context of modified gravity spacetime, α is a free parameter to whom we assign various values. When $\alpha = 0$, the scenario corresponds to the Schwarzschild case. As the value of α increases, μ_{pt} increase. The tangential magnification of the secondary image (μ_{sr}) is plotted against $\mathcal{D}$. The values of μ_{sr} decreases when we increase the value of α. Second Row: The total magnification of the primary images is plotted against $\mathcal{D}$. This total magnification increases as both $\mathcal{D}$ and α increase.

Figure 3.10: First Row: The tangential magnification for the secondary image (μ_{st}) is plotted against $\mathcal{D}$ which represents the ratio of observer-lens distance to lens-source distance. When $\alpha = 0$, the scenario corresponds to the Schwarzschild case. As the value of α increases, μ_{st} increase. Second Row: The radial magnification of the secondary image (μ_{sr}) is plotted against D. The μ_{sr} decreases when α and D increases. Third Row: The total magnification of secondary images is plotted against $\mathcal{D}$. This total magnification increases as both $\mathcal{D}$ and α increase.
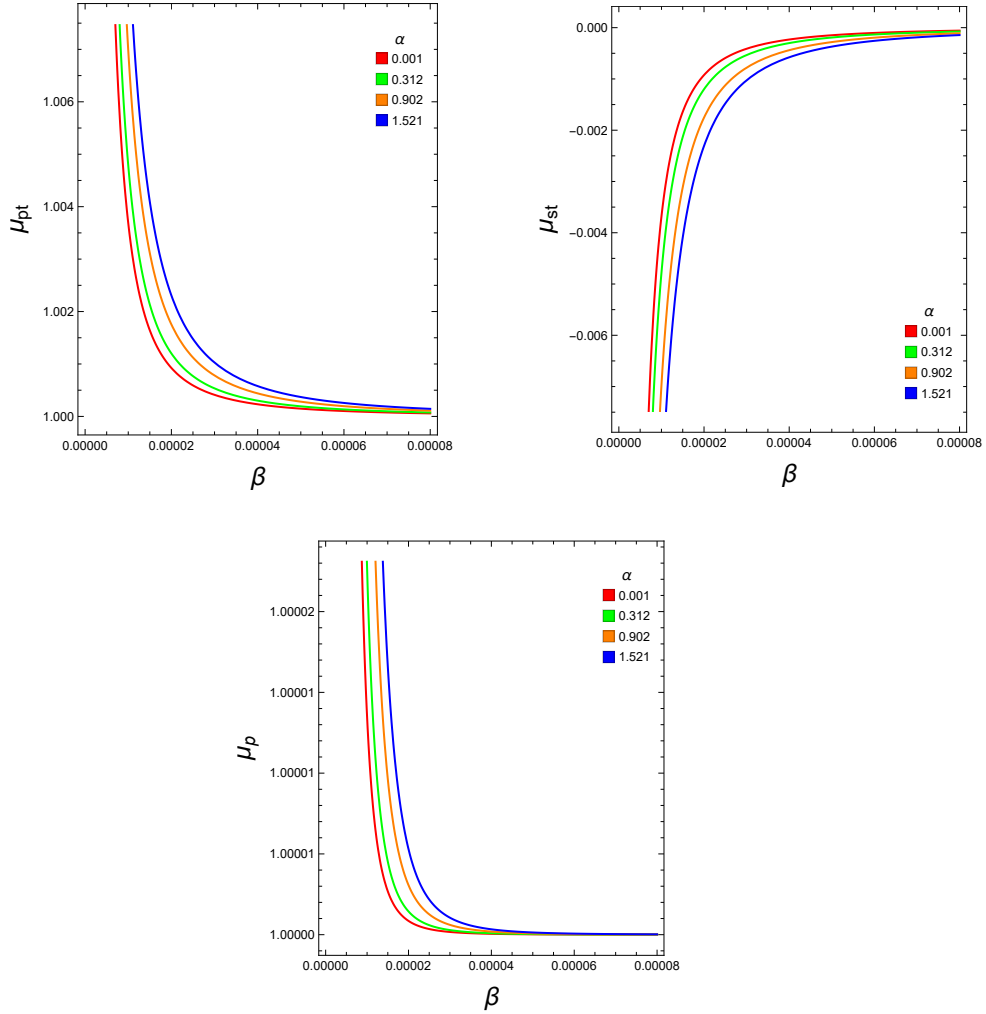
Figure 3.11: 1st Row: The tangential magnification for the primary image (μ_{pt}) is plotted against β which represents the angular separation of the source. As the value of α increases, μ_{st} increases. Second Row: The radial magnification of the primary (μ_{pr}) image is plotted against β. The value of μ_{pr} decreases with an increase in β and α. Third Row: The total magnification of the primary images is plotted against β. This total magnification increases as both β and α increase.
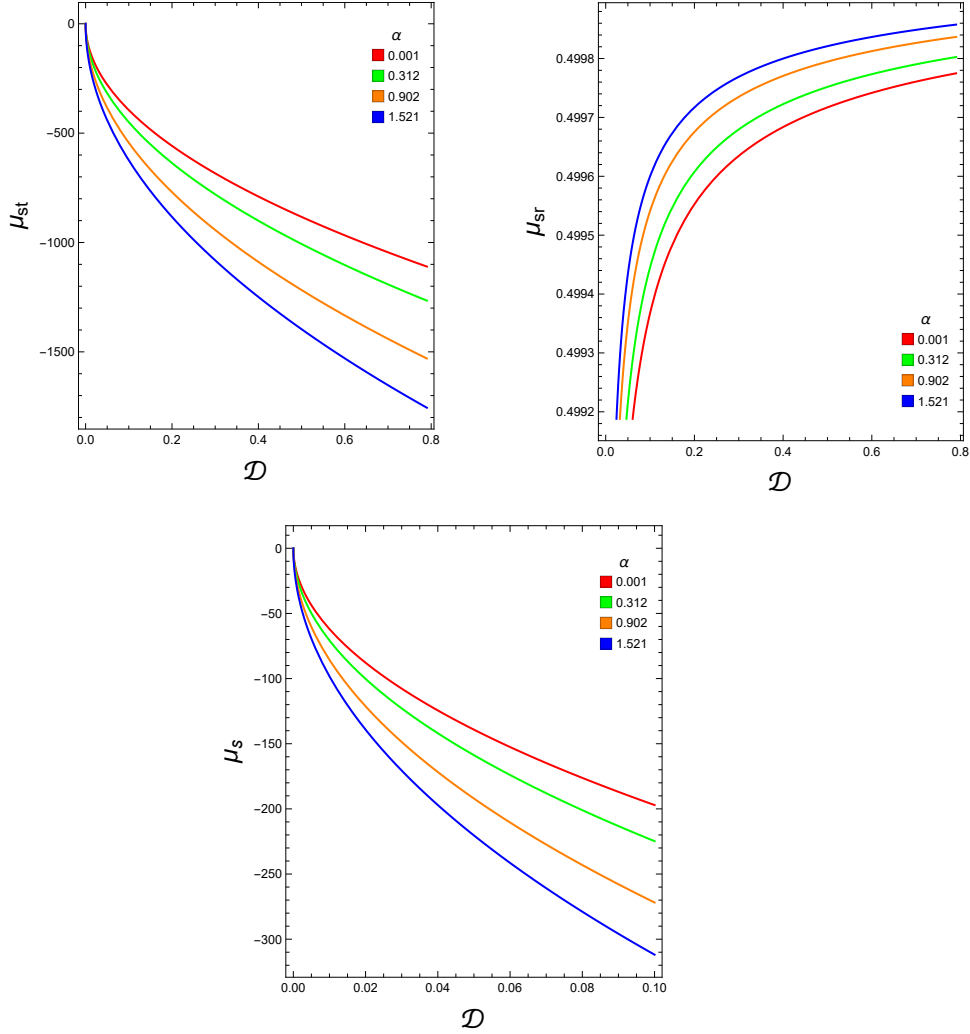
61
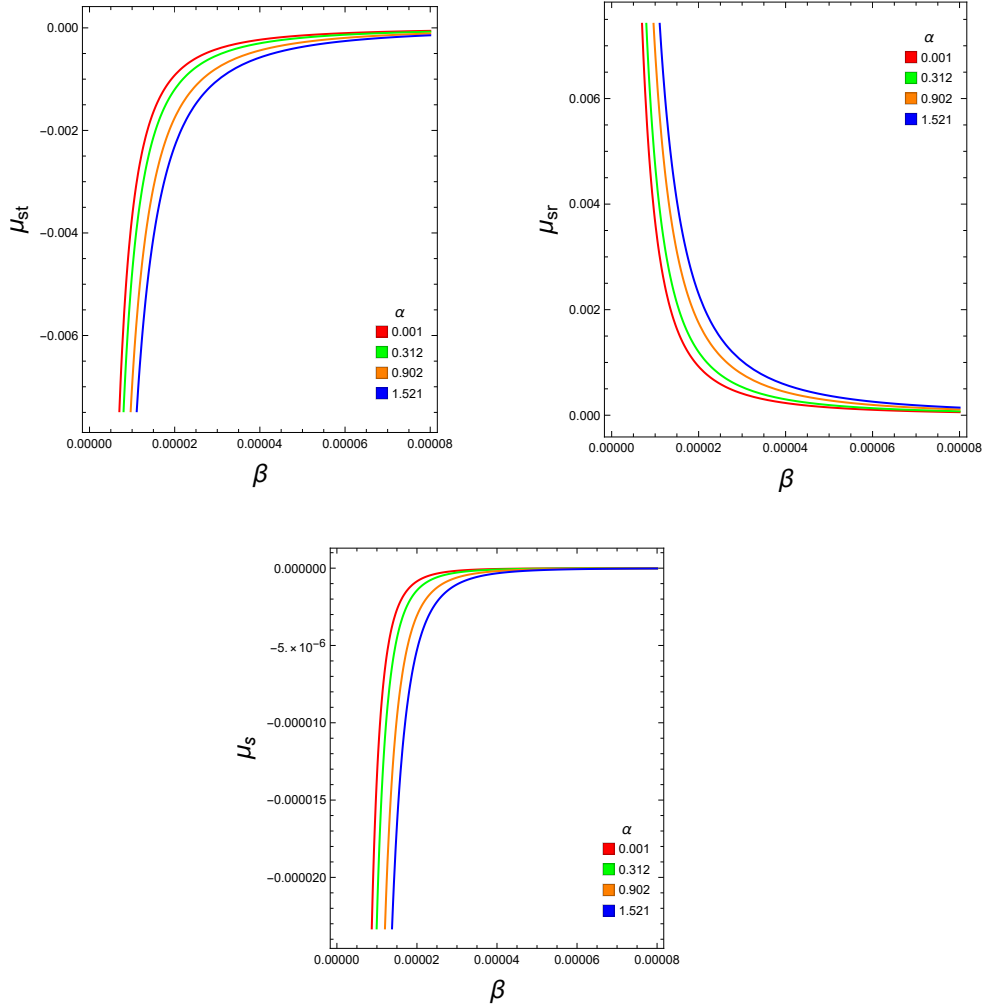
Figure 3.12: 1st Row: The tangential magnification for the secondary image (μ_{st}) is plotted against β which represents the angular separation of the source. As the value of α increases, μ_{st} increases. Second Row: The radial magnification of the secondary image (μ_{sr}) is plotted against β. The value of μ_{pr} decreases with an increase in β and α, while μ_{sr} also decreases under the same conditions. Third Row: The total magnification of the secondary images is plotted against β. This total magnification increases as β and α increases.
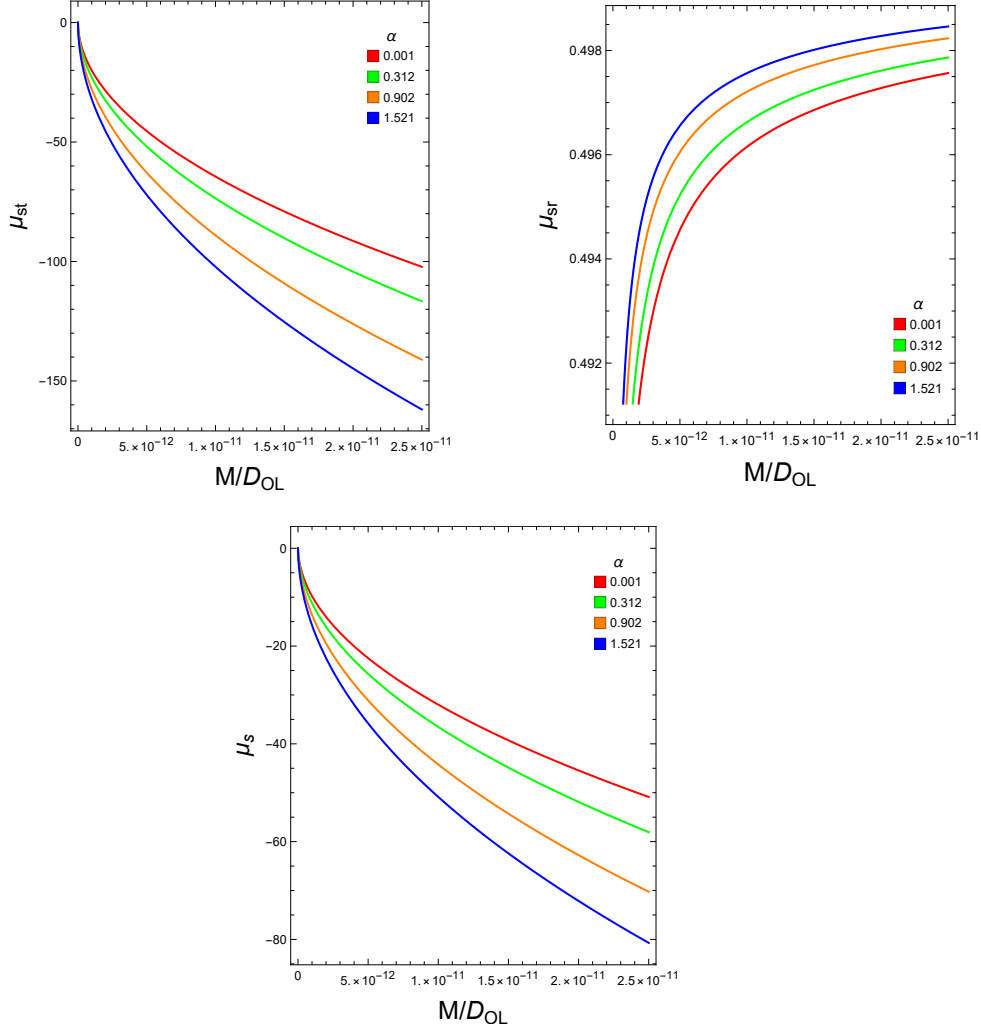
Figure 3.13: The ratio M/D_{ol} has given different values to predict the nature of tangential and radial magnification in modified gravity and plots are given here. 1st row: The tangential magnification for the secondary image (μ_{st}) is plotted against M/D_{ol} which represents a ratio of massive body and observer-lens distance. As the value of M/D_{ol} increases, μ_{st} increases. Second Row: The radial magnification of the secondary image (μ_{sr}) is plotted against M/D_{ol}. The μ_{sr} value decreases under the when M/D_{ol} and α increases. Third Row: The total magnification of secondary images is plotted against M/D_{ol}. This total magnification increases as both D and α increase.

Figure 3.14: The ratio M/D_{ol} has given different values to predict the nature of tangential and radial magnification in modified gravity and plots are given here. 1st row: The tangential magnification for the primary image (μ_{pt}) is plotted against M/D_{ol} which represents a ratio of massive body and observer-lens distance. As the value of M/D_{ol} increases, μ_{pt} increases. Second Row: The radial magnification of the secondary image (μ_{pr}) is plotted against M/D_{ol}. The μ_{pr} value decreases under the when M/D_{ol} and α increases. Third Row: The total magnification of the primary image is plotted against M/D_{ol}. This total magnification increases as both M/D_{ol} and α increase.
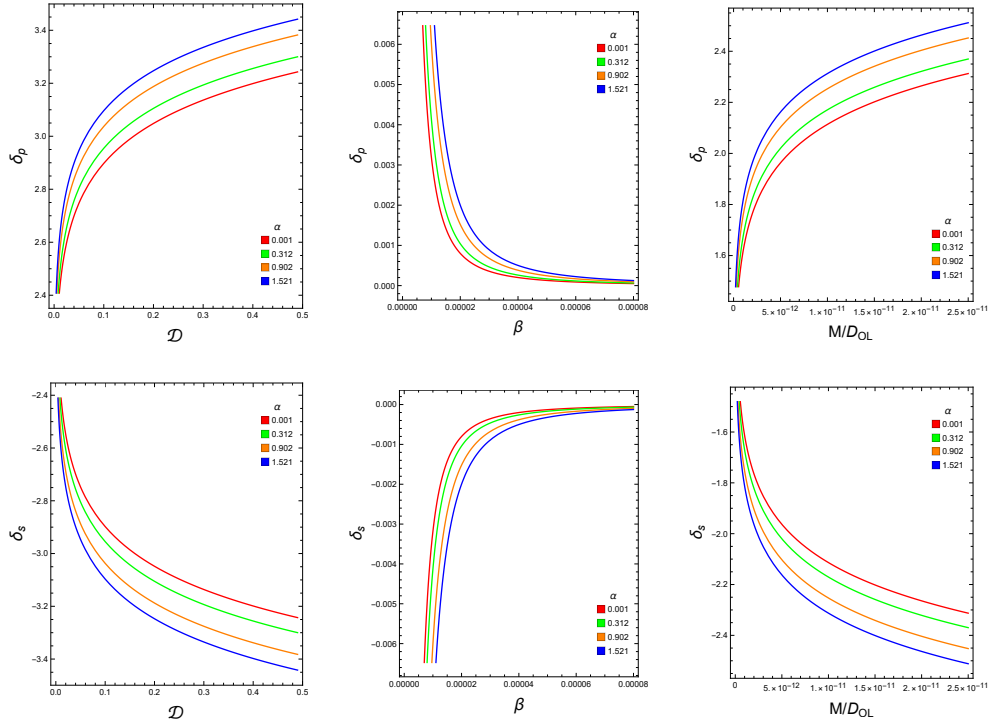
Figure 3.15: Logarithmic distortion versus $\mathcal{D}$, β and M/D_{ol} for images is plotted here for different values of α. 1st row: Logarithmic distortion is plotted against the mentioned parameters. Distortion increases with an increase in all parameters. Second Row: The plots of δ against the above parameters are given for secondary images. They are also representing an increase in distortion.

Chapter 4

Weak Deflection Angle of Strongly Null Naked Singularity

The weak deflection angle is important in gravitational lensing theory because it helps explain how light bends around enormous objects that lack a typical event horizon, such as strongly null naked singularities. While black holes and compact objects with well-defined horizons have traditionally received a lot of attention. Recent theoretical developments have highlighted the importance of studying singularities that lack event horizon, and exhibit extreme gravitational effects on light passing by. Strongly null naked singularities are rare instances in which spacetime curvature is strong enough to alter photon trajectories but lacks the enclosing border as in black holes. This chapter explores the weak deflection angle of a strongly null naked singularity. We use Gibbons and Werner's approach to find weak deflection angles as done in chapter 3. The line element introduced by Joshi for a strongly null naked singularity[1] will be used in this analysis.

The line element of naked singularity is

$$ds^2 = -\frac{dt^2}{\left(1 + \frac{M}{r}\right)^2} + \left(1 + \frac{M}{r}\right)^2 dr^2 + r^2 d\Omega^2 \tag{4.1}$$

Here, the angular part of the metric is:

$$d\Omega^2 = d\theta^2 + \sin^2\theta \, d\phi^2.$$

---

[1]1A strongly null naked singularity is characterized by the absence of both a photon sphere and an event horizon [46].

Without losing any generality, we set $\theta = \frac{\pi}{2}$, which simplifies the angular part to:

$$d\Omega^2 = d\phi^2.$$

Now, using the null geodesic condition ($ds^2 = 0$), we can write the optical metric as:

$$ds^2 = -\frac{dt^2}{\left(1 + \frac{M}{r}\right)^2} + \left(1 + \frac{M}{r}\right)^2 dr^2 + r^2 d\phi^2.$$

Setting $ds^2 = 0$ for null geodesics gives:

$$-\frac{dt^2}{\left(1 + \frac{M}{r}\right)^2} + \left(1 + \frac{M}{r}\right)^2 dr^2 + r^2 d\phi^2 = 0.$$

Rearranging, we obtain:

$$dt^2 = \left(1 + \frac{M}{r}\right)^4 dr^2 + r^2 \left(1 + \frac{M}{r}\right)^2 d\phi^2. \tag{4.2}$$

(4.2) is an optical metric and we can express it generally as

$$dt^2 = \overline{g}_{rr} dr^2 + \overline{g}_{\phi\phi} d\phi^2, \tag{4.3}$$

here

$$\overline{g}_{rr} = \left(1 + \frac{M}{r}\right)^4, \qquad \overline{g}_{\phi\phi} = r^2 \left(1 + \frac{M}{r}\right)^2.$$

(4.1)) is asymptotically flat as it satisfies the condition defined in (2.20). So, we will apply the Gauss-Bonnet theorem to find the weak deflection angle of naked singularity spacetime. For any asymptotically flat spacetime [55]

$$\hat{\alpha} = -\int_0^\pi \int_{r_\gamma}^\infty \mathcal{K} dS. \tag{4.4}$$

Here, $\mathcal{K}$ is the Gaussian curvature of the surface and dS is the areal element defined as $dS = \sqrt{\overline{g}_{rr}\overline{g}_{\phi\phi}} dr d\phi$. The value of Gaussian curvature is calculated by using (1.6)

$$
\begin{aligned}
K &= -\frac{1}{\sqrt{r^2 \left(1 + \frac{M}{r}\right)^4}} \left(\frac{\partial}{\partial r}\left(\frac{1}{\sqrt{\left(1 + \frac{M}{r}\right)^4}}\right)\right), \\
&= -\frac{2M}{r^3 \left(1 + \frac{M}{r^2}\right)^6}.
\end{aligned}
\tag{4.5}
$$

The expression for the areal element

$$dS = r \left(1 + \frac{M}{r}\right)^3 dr d\phi. \tag{4.6}$$

So, the weak deflection angle is calculated by using (4.5), (4.6) into (4.4), we get

$$\hat{\alpha} = \int_0^\pi \int_{\frac{b}{\sin\phi}}^\infty \frac{2M}{r^2 \left(1 + \frac{M}{r^2}\right)^3} dr d\phi. \tag{4.7}$$

The evaluation of the first integral gives

$$\hat{\alpha} = \int_0^\pi \frac{M^2 \sin^2\phi}{b^2 \left(\frac{M\sin\phi}{b} + 1\right)^2} d\phi + \int_0^\pi \frac{M^2 \sin\phi}{b \left(\frac{M\sin\phi}{b} + 1\right)^2} d\phi. \tag{4.8}$$

By using Mathematica, the final expression of the weak deflection angle is

$$\begin{aligned}
\hat{\alpha} = &\frac{2bM}{b^2 - M^2} - \frac{M^2\pi}{b^2 - M^2} + \frac{b^2\pi}{b^2 - M^2} - \frac{b^3\pi}{(b^2 - M^2)^{3/2}} \\
&+ \frac{2b^3}{(b^2 - M^2)^{3/2}} \arctan\left(\sqrt{\frac{M}{b^2 - M^2}}\right) + O(M^3).
\end{aligned} \tag{4.9}$$

Using the identity $\arctan\left(\frac{1}{x}\right) = \frac{\pi}{2} - \arctan(x)$, we get

$$\hat{\alpha} = \frac{2bM}{b^2 - M^2} - \pi - \frac{2b^3}{(b^2 - M^2)^{3/2}} \arctan\left(\sqrt{\frac{b^2}{M^2} - 1}\right) + O(M^3). \tag{4.10}$$

The weak deflection angle of a strongly null naked singularity is the same as its strong deflection angle [46]. This is a significant characteristic of this specific naked singularity. This might suggest that the spacetime curvature around the lensing object does not change significantly across different impact parameters and portrays a unique behavior of the gravitational field in that spacetime, where light deflection remains relatively stable regardless of the impact parameter.

Chapter 5

Summary and Conclusion

In this thesis, we have explored various aspects of gravitational lensing, focusing on strong and weak gravitational fields and comparing different astrophysical objects' effects on light deflection. The introductory chapter provides a comprehensive overview of gravitational lensing, its significance in astrophysics, and the historical development of the field. The phenomenon's basic principles and the equations governing light deflection in gravitational fields are discussed, setting the stage for detailed analyses in subsequent chapters.

Chapter 2 delves into the strong bending angle of naked singularities and their unique characteristics. It examines the strong deflection angle in space-times with a photon sphere and ultracompact objects. The study highlights the differences between black holes and horizon-less ultracompact objects in producing relativistic images. Black holes generate relativistic images only outside their photon circles, whereas horizon-less ultracompact objects can produce additional relativistic images within their photon sphere radius. This chapter presents an analytical technique for significant gravitational lensing from ultra-compact objects, contrasting it with the black hole scenarios reported by Bozza [53].

Chapter 3 investigates several critical aspects of spacetime within the framework of Modified Gravity (MOG). It begins with the line element of spacetime in MOG, laying the foundation for understanding spacetime structure under this theory. The chapter then analyzes the weak deflection angle, exploring light bending in weak gravitational fields, followed by the study of the strong deflection angle in strong gravitational fields near massive objects like black holes. The analysis includes identifying observable quantities in strong gravity, magnification and distortion parameters, and measurable effects in the weak field limit.

This thesis presents a thorough investigation of gravitational lensing phe-

nomena in various astrophysical contexts, including naked singularities, ultracompact objects, and scenarios within Modified Gravity (MOG). The analytical techniques developed for studying significant gravitational lensing in ultracompact objects provide new insights, expanding our understanding beyond traditional black hole models. The comparative analysis of black holes and horizon-less ultracompact objects enhances our comprehension of relativistic image formation and the unique characteristics of different gravitational lenses.

The exploration of Modified Gravity (MOG) offers a fresh perspective on spacetime structure and light deflection in both weak and strong gravitational fields. The findings contribute to the broader understanding of gravitational lensing, emphasizing the importance of considering alternative theories of gravity. By identifying observable parameters and analyzing their implications, this research provides valuable tools for future observational studies and theoretical developments in the field of gravitational lensing.

Overall, this thesis emphasizes the complexity and variety of gravitational lensing processes, emphasizing the necessity for further investigation of various gravitational models and astrophysical objects. The findings of this study set the path for future advances in understanding the interaction of gravity and light, leading to the discovery of new astrophysical phenomena and the refinement of existing theories.

Bibliography

[1] J. Kormendy and L. C. Ho, "Coevolution (or not) of supermassive black holes and host galaxies," *Annual Review of Astronomy and Astrophysics*, vol. 51, no. 1, pp. 511–653, 2013.

[2] A. Einstein *et al.*, "Zur elektrodynamik bewegter körper," *Annalen der physik*, vol. 17, no. 10, pp. 891–921, 1905.

[3] A. Einstein, "Does the Inertia of a body depend upon its energy-content," *Annalen der physik*, vol. 18, no. 13, pp. 639–641, 1905.

[4] L. A. Bauer, "Resume of observations concerning the solar eclipse of may 29, 1919, and the einstein effect," *Science*, vol. 51, no. 1317, pp. 301–311, 1920.

[5] J. Earman and C. Glymour, "Relativity and eclipses: The british eclipse expeditions of 1919 and their predecessors," *Historical Studies in the Physical Sciences*, vol. 11, no. 1, pp. 49–85, 1980.

[6] I. I. Shapiro, "A century of relativity," *Reviews of Modern Physics*, vol. 71, no. 2, p. S41, 1999.

[7] R. Sharma, "Gravitational lensing and concrete evidence of dark matter," *International Journal of Research in Engineering Technology and Management*, vol. 2, no. 5, 2014.

[8] G. Lensing, "Strong, weak, micro," in *Proceedings of the Gravitational Lensing Conference*, Springer, 2006.

[9] S. Refsdal and J. Surdej, "Gravitational lensing," *Highlights of Astronomy*, vol. 9, pp. 3–32, 1992.

[10] D. Roberts, P. Greenfield, and B. Burke, "The double quasar 0957+ 561: a radio study at 6-centimeters wavelength," *Science*, vol. 205, no. 4409, pp. 894–896, 1979.

[11] J. Zensus, M. Cohen, and S. Unwin, "The parsec-scale jet in Quasar 3c 345," *Astrophysical Journal, Part 1 (ISSN 0004-637X), vol. 443, no. 1, p. 35-53*, vol. 443, pp. 35–53, 1995.

[12] J. Narlikar and K. Subramanian, "A Single Exhaust Model for Backward emission in doppler quasars," *Astrophysical Journal, Part 1 (ISSN 0004-637X), vol. 273, Oct. 1, 1983, p. 44-57.*, vol. 273, pp. 44–57, 1983.

[13] J. Lehar, J. Hewitt, D. Roberts, and B. Burke, "The radio time delay in the double quasar 0957+ 561," *Astrophysical Journal, Part 1*, vol. 384, pp. 453–466, 1992.

[14] W. C. Keel, "From shifting stars to multiple quasars," *The Sky at Einstein's Feet*, pp. 97–119, 2006.

[15] K. Akiyama, A. Alberdi, W. Alef, K. Asada, R. Azulay, A.-K. Baczko, D. Ball, M. Baloković, J. Barrett, D. Bintley, *et al.*, "First M87 Event Horizon Telescope results. VI. the shadow and mass of the central black hole," *The Astrophysical Journal Letters*, vol. 875, no. 1, p. L6, 2019.

[16] K. Jusufi, M. Jamil, P. Salucci, T. Zhu, and S. Haroon, "Black hole surrounded by a dark matter halo in the M87 galactic center and its identification with shadow images," *Physical Review D*, vol. 100, no. 4, p. 044012, 2019.

[17] J. W. Moffat, "A new nonsymmetric gravitational theory," *Physics Letters B*, vol. 355, no. 3-4, pp. 447–452, 1995.

[18] J. Moffat, "Gravitational theory, galaxy rotation curves and cosmology without dark matter," *Journal of Cosmology and Astroparticle Physics*, vol. 2005, no. 05, p. 003, 2005.

[19] J. W. Moffat, "Scalar–tensor–vector gravity theory," *Journal of Cosmology and Astroparticle Physics*, vol. 2006, no. 03, p. 004, 2006.

[20] J. Moffat and V. T. Toth, "Fundamental parameter-free solutions in modified gravity," *Classical and Quantum Gravity*, vol. 26, no. 8, p. 085002, 2009.

[21] J. Moffat, "Modified Gravity black holes and their observable shadows," *The European Physical Journal C*, vol. 75, no. 3, p. 130, 2015.

[22] J.Moffat, "Black holes in Modified Gravity (MOG)," *The European Physical Journal C*, vol. 75, no. 4, p. 175, 2015.

[23] J. R. Mureika, J. W. Moffat, and M. Faizal, "Black hole thermodynamics in Modified Gravity (MOG)," *Physics Letters B*, vol. 757, pp. 528–536, 2016.

[24] J. Moffat, "LIGO GW150914 and GW151226 Gravitational wave detection and generalized gravitation theory," *Physics Letters B*, vol. 763, pp. 427–433, 2016.

[25] L. Manfredi, J. Mureika, and J. Moffat, "Quasinormal modes of Modified Gravity (MOG) Black Holes," *Physics Letters B*, vol. 779, pp. 492–497, 2018.

[26] J. Moffat, "Modified Gravity (MOG), cosmology and black holes," *Journal of Cosmology and Astroparticle Physics*, vol. 2021, no. 02, p. 017, 2021.

[27] Z. Yousaf, K. Bamba, M. Bhatti, and U. Farwa, "Quasi static evolution of compact objects in Modified Gravity," *General Relativity and Gravitation*, vol. 54, no. 1, p. 7, 2022.

[28] U. Farwa, Z. Yousaf, and M. Bhatti, "A measure of complexity for axial self-gravitating static fluids," *Physica Scripta*, vol. 97, no. 10, p. 105307, 2022.

[29] P. Chaturvedi, U. Kumar, U. Thattarampilly, and V. Kakkat, "Exact rotating black hole solutions for $f(R)$ gravity by modified Newman Janis algorithm," *The European Physical Journal C*, vol. 83, no. 12, p. 1124, 2023.

[30] J.Moffat, "Regular Rotating MOG Dark Compact Object," *The European Physical Journal C*, vol. 81, pp. 1–6, 2021.

[31] K. Virbhadra, "Distortions of images of Schwarzschild lensing," *Physical Review D*, vol. 106, no. 6, p. 064038, 2022.

[32] S. M. Carroll, *Spacetime and geometry*. Cambridge University Press, 2019.

[33] R. M. Wald, *General relativity*. University of Chicago press, 2010.

[34] H. Arakida and M. Kasai, "Effect of the cosmological constant on the bending of light and the cosmological lens equation," *Physical Review D*, vol. 85, no. 2, p. 023006, 2012.

73

[35] A. Ishihara, Y. Suzuki, T. Ono, T. Kitamura, and H. Asada, "Gravitational bending angle of light for finite distance and the Gauss-Bonnet theorem," *Physical Review D*, vol. 94, no. 8, p. 084015, 2016.

[36] A. Ishihara, Y. Suzuki, T. Ono, and H. Asada, "Finite-distance corrections to the gravitational bending angle of light in the strong deflection limit," *Physical Review D*, vol. 95, no. 4, p. 044017, 2017.

[37] W. Klingenberg, *A course in Differential Geometry*, vol. 51. Springer Science & Business Media, 2013.

[38] R. C. Pantig and E. T. Rodulfo, "Weak deflection angle of a dirty black hole," *Chinese Journal of Physics*, vol. 66, pp. 691–702, 2020.

[39] E. Kreyszig, *Differential geometry*. Dover Publications, 2013.

[40] M. P. Do Carmo, *Differential geometry of curves and surfaces: revised and updated second edition*. Courier Dover Publications, 2016.

[41] V. Bozza, "Comparison of approximate gravitational lens equations and a proposal for an improved new one," *Physical Review D*, vol. 78, no. 10, p. 103005, 2008.

[42] K. S. Virbhadra and G. F. Ellis, "Schwarzschild black hole lensing," *Physical Review D*, vol. 62, no. 8, p. 084003, 2000.

[43] J. P. DeAndrea and K. M. Alexander, "Negative time delay in strongly naked singularity lensing," *Physical Review D*, vol. 89, no. 12, p. 123012, 2014.

[44] A. Y. Bin-Nun, "Relativistic images in Randall-Sundrum II braneworld lensing," *Physical Review D—Particles, Fields, Gravitation, and Cosmology*, vol. 81, no. 12, p. 123011, 2010.

[45] J. Wambsganss, "Gravitational lensing in astronomy," *Living Reviews in Relativity*, vol. 1, pp. 1–74, 1998.

[46] S. Paul, "Strong gravitational lensing by a strongly naked null singularity," *Physical Review D*, vol. 102, no. 6, p. 064045, 2020.

[47] K. Landsman, "Singularities, black holes, and cosmic censorship: A tribute to roger penrose," *Foundations of Physics*, vol. 51, pp. 1–38, 2021.

74

[48] A. B. Joshi, D. Dey, P. S. Joshi, and P. Bambhaniya, "Shadow of a naked singularity without photon sphere," *Physical Review D*, vol. 102, no. 2, p. 024022, 2020.

[49] V. Bozza, "Gravitational lensing in the strong field limit," *Physical Review D*, vol. 66, no. 10, p. 103001, 2002.

[50] N. Tsukamoto, "Deflection angle in the strong deflection limit in a general asymptotically flat, static, spherically symmetric spacetime," *Physical Review D*, vol. 95, no. 6, p. 064035, 2017.

[51] S. Dodelson, *Gravitational lensing.* Cambridge University Press, 2017.

[52] R. Shaikh, P. Banerjee, S. Paul, and T. Sarkar, "Analytical approach to strong gravitational lensing from ultra-compact objects," *Physical Review D*, vol. 99, no. 10, p. 104040, 2019.

[53] V. Bozza, S. Capozziello, G. Iovane, and G. Scarpetta, "Strong field limit of Black Hole gravitational lensing," *General Relativity and Gravitation*, vol. 33, pp. 1535–1548, 2001.

[54] E. Ayon-Beato and A. Garcia, "Regular Black Hole in general relativity coupled to nonlinear electrodynamics," *Physical review letters*, vol. 80, no. 23, p. 5056, 1998.

[55] G. Gibbons and M. Werner, "Applications of the Gauss-Bonnet theorem to gravitational lensing," *Classical and Quantum Gravity*, vol. 25, no. 23, p. 235009, 2008.

[56] H. Arakida, "Light deflection and Gauss-Bonnet theorem: definition of total deflection angle and its applications," *General Relativity and Gravitation*, vol. 50, no. 5, p. 48, 2018.

[57] V. Bozza, "Gravitational lensing by black holes," *General Relativity and Gravitation*, vol. 42, pp. 2269–2300, 2010.

[58] V. Bozza and L. Mancini, "Time delay in black hole gravitational lensing as a distance estimator," *General Relativity and Gravitation*, vol. 36, pp. 435–450, 2004.